

# Development of control strategy of DC-DC converter for optimal operation of PV powered Electrolyser

Thesis report

Avinash Kalloe





# Development of control strategy of DC-DC converter for optimal operation of PV powered Electrolyser

Thesis report

by

Avinash Kalloe

to obtain the degree of Master of Science  
at the Delft University of Technology,  
to be defended publicly on Tuesday August 24, 2021 at 1:00 PM.

|                   |  |
|-------------------|--|
| Student number:   | 4574427  |
| Project duration: | November 16, 2020 – August 24, 2021                |
| Thesis committee: | Prof. dr. ir. A. Smets, TU Delft, Chairman         |
|                   | Dr. Z. Ahmad, TU Delft, Daily supervisor           |
|                   | Dr. H. Ziar, TU Delft, supervisor                  |
|                   | Dr. A. Lekic, TU Delft, External member            |
|                   | Prof. C. van Kruijsdijk, Shell BV, External member |

*This thesis is confidential and cannot be made public until December 31, 2021.*

An electronic version of this thesis is available at <http://repository.tudelft.nl/>.



# Preface

This thesis has been produced as a final work to fulfill my Master in Science program in Electrical Power Engineering at the Delft University of Technology. I am extremely happy with the experience and knowledge I gained from this Msc.thesis project. I met amazing people that contributed towards my development as a person and as an engineer. First of all, I would like to express my immense gratitude towards my thesis daily supervisor, Dr. Zameer Ahmad. His guidance was of great importance in aiding me towards the completion of this project. He was always available for my questions, doubts & a wonderful chat. His passion for the subject and determination are inspiring and motivating. I would like to also thank Dr. Hesam Ziar for his valuable input and advice.

I cannot express how happy i am for my family and friends who have been encouraging and were always there for me when I needed them. The care and support I received from my parents and my sisters Sudarshini, Davini & Parmodini were vital to my progression in the master program. My Brothers from Suriname, Irash, Ravish, Darshan & Tante Shaan for their support. great company and amazing food. My dearest friends at Delft, Mohammed El-Hayek, Serge Saaybi, Habib Elkassis, Aschraf Gardouh and Belkasssem Becetti who I was extremely lucky to meet on, they made the past months bearable and fun. Many thanks to Gym & Bike Buddy & friend for life Henk Janse. and to my day one group of Laura Croes and Lynrick Wix, Thank you for the fun times and eternal friendship. Lastly, I would like to thank the staff of the InHolland university of applied sciences for allowing students to access their building during the lockdown and use their facilities without requesting permission.

*Avinash Kalloe  
Delft, August 2021*



# Abstract

With the current need of implementing renewable energy sources to combat climate change, significant developments are being done into storage options for these intermittent energy sources. Green Hydrogen can be produced by the connection of a renewable energy source to an electrolyser which produces hydrogen, in this project the Photovoltaic (PV) System is indirectly connected to the electrolyser as this gives the ability to control the different systems and also flexibility in sizing the different systems. Several different dc/dc converters are simulated in Matlab Simulink and compared to each other while also taking into account the project requirements.

First, an overview of the project is presented after which the main idea of the thesis is presented in which the dc/dc converters are selected for optimal operation of the system. Two converter are selected based on simulations and mathematical calculations (Component sizes, Voltage ripple & Current ripple), for the Maximum Power Tracking converter (Connected to the PV system) the buck-boost converter was selected. This was because of its ability to fully track the Current-Voltage curve of a PV system. And for the connection to the Electrolyser system a 3-level Interleaved Buck converter was selected, because of its increased reliability to be able to continue working after a power electronic switch failure. With the PV system maximum power point being between 580-582 V (depending on the irradiance) and a Electrolyser voltage range between 210-260 V, the voltage needed to be reduced.

After selecting the different converters a control system was modelled and simulated, this is to optimize and control the working points of the PV-Electrolyser system. This control system works on the idea of matching the electrolyser load working point to the available PV power from the input.

This control algorithm selects the right reference voltage which then goes into a voltage controller to ensure the correct voltage is at the output for the electrolyser load. This control algorithm was modelled and simulated in Matlab simulink and tested against different changing inputs (Changing the irradiance & electrolyser temperature). Furthermore the controller was checked for several different stepsizes and time delays (accounting for external effects) and the optimal combination was found to be a stepsize of 0.1V and timedelay of 1ms which gave an Converter+algorithm efficiency of 98.42%. The results demonstrate the controllers ability to correctly follow the irradiance pattern and electrolyser temperature changes.





# Contents

|  |    |
|--|----|
| Abstract   | v  |
| 1 Introduction   | 1  |
| 1.1 Background   | 1  |
| 1.2 Motivation   | 1  |
| 1.3 PV-electrolyser application                        | 1  |
| 1.3.1 PV system  | 1  |
| 1.3.2 Electrolyser                                     | 3  |
| 1.3.3 DC/DC converter                                  | 4  |
| 1.4 Research goals                                     | 5  |
| 1.5 Report outline                                     | 5  |
| 2 DC-DC converters                                     | 7  |
| 2.1 Non-isolated DC-DC converters                      | 8  |
| 2.1.1 Boost converter                                  | 8  |
| 2.1.2 Buck converter                                   | 8  |
| 2.1.3 Buck-Boost converter                             | 9  |
| 2.1.4 Cuk converter                                    | 10 |
| 2.1.5 Sepic converter                                  | 12 |
| 2.1.6 Interleaved Buck Converter                       | 12 |
| 2.2 Isolated DC-DC converters                          | 13 |
| 2.2.1 Flyback converter                                | 13 |
| 2.2.2 Forward converter                                | 14 |
| 2.2.3 Push-Pull converter                              | 14 |
| 2.2.4 Half-Bridge converter                            | 16 |
| 2.2.5 Full-Bridge converter                            | 16 |
| 2.3 SIMULINK results & comparison                      | 18 |
| 3 Electrolyser   | 25 |
| 3.1 Alkaline electrolysis                              | 25 |
| 3.2 Proton exchange membrane (PEM) electrolysis        | 25 |
| 3.3 Solid oxide high temperature electrolysis          | 26 |
| 3.4 Selected electrolyser: Alkaline electrolyser model | 26 |
| 4 Control systems                                      | 29 |
| 4.1 Control algorithms                                 | 29 |
| 4.1.1 Maximum power point tracking                     | 30 |
| 4.1.2 Control algorithm: Power matching                | 31 |
| 4.2 Control algorithm SIMULINK simulation              | 32 |
| 4.2.1 Two converter simulation                         | 33 |
| 4.2.2 Varying Irradiance & constant Temperature        | 33 |
| 4.2.3 Constant Irradiance & Varying Temperature        | 35 |
| 4.2.4 Varying Irradiance & Varying Temperature         | 35 |
| 4.3 PV system variation & day irradiance model         | 36 |
| 4.3.1 Winter & Summer day Delft                        | 36 |
| 4.3.2 Clear day simulation                             | 36 |
| 5 Conclusion & future recommendations                  | 45 |
| 5.1 Conclusions  | 45 |
| 5.2 Recommendations                                    | 45 |



# 1

## Introduction

### 1.1. Background

In the last few years the current energy transition of the world from fossil fuels to more renewable energy sources such as wind, hydro, solar, and biomass has become more important than ever. And with the world population still growing and the energy needs increasing yearly (approximately 18% in 2018 to 24 % by 2040) more renewable energy sources are needed to combat climate change and reduce carbon emissions [1]. But due to these renewable sources being intermittent energy sources as seen in Figure 1.1 (daily and seasonal variations) more research is being done into the different options for storing this energy [2].

### 1.2. Motivation

Several storage options include batteries, flywheels, and hydrogen storage. In Figure 1.2 different energy storage options are shown comparing their capacity and discharge time. Smaller power systems use batteries as they supply for several hours up to days as seen in Figure 1.2 [5]. Using batteries as energy storage option gives several issues such as limited charge rates, maintenance requirements and short lifetimes that are also dependent on the number and depth of discharge cycles [5]. Bigger power systems are usually connected with diesel generators that provide the necessary power when the renewable energy sources lack the required amount of energy. Also, these larger power systems have a high reliance on the diesel generator and less usage of renewable energy not helping the case in working towards a more renewable world [5]. Renewable energy storage in the form of hydrogen may overcome the inherent weakness of battery based energy storage systems like physical size, limited life span, initial capital cost of the battery bank directly connected with maintenance, and battery disposal issues [6]. Figure 1.2 shows that hydrogen has a high energy density and also is able to supply energy for weeks/months depending on its size which makes it a good option for energy storage. The idea of this project is to connect a Photovoltaic system (PV system) to an electrolyser which will make the hydrogen that can be used for creating the required energy in a power system. This connection will be made by making use of power electronics and a control system that will be build to optimize the working points and efficiency of the system. The different subsystems will all be build and simulated in Matlab Simulink.

### 1.3. PV-electrolyser application

Figure 1.3 shows the main layout of the whole system consisting on the renewable energy source a PV plant which is connected to an electrolyser through the use of power electronics converters, these DC-DC converters are controlled through a control system which has input signals from both the PV side and the electrolyser side. This control system is needed to run the PV-electrolyser application as efficient as possible.

#### 1.3.1. PV system

The PV system used in Matlab Simulink is based on the one-diode model, which consists of 4 components that can be seen in Figure 1.4

$$I_d = I_O \left[ \exp\left(\frac{V_d}{V_t}\right) - 1 \right] \quad (1.1)$$

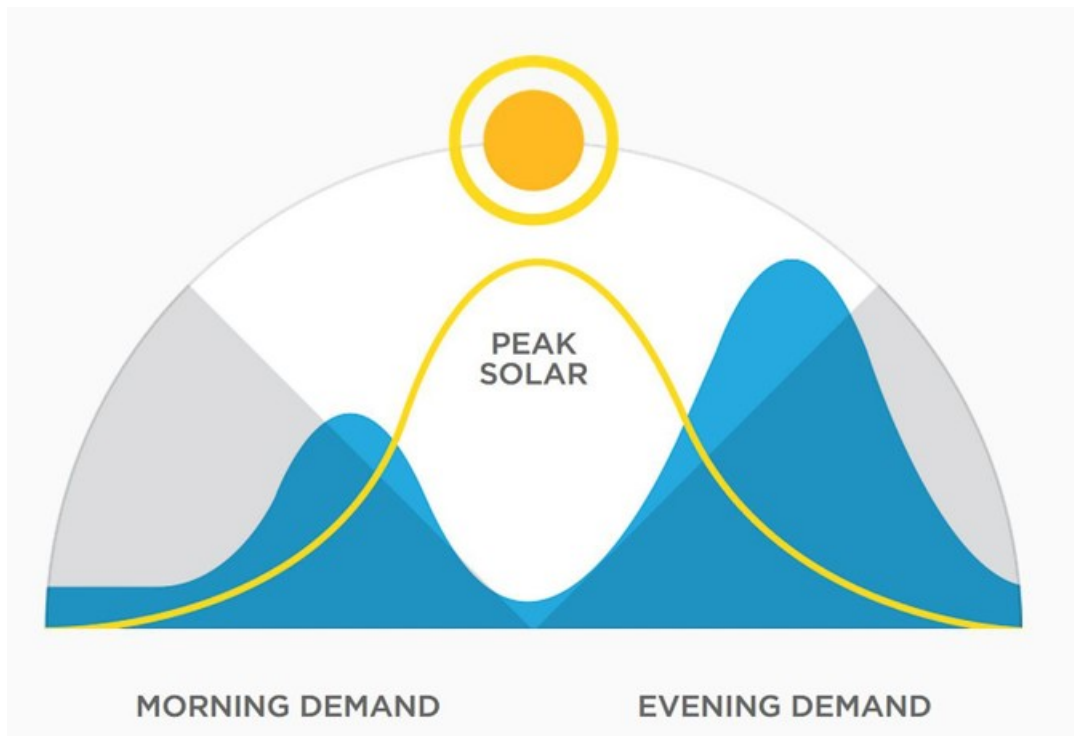


Figure 1.1: load demand vs daily solar irradiance [3]

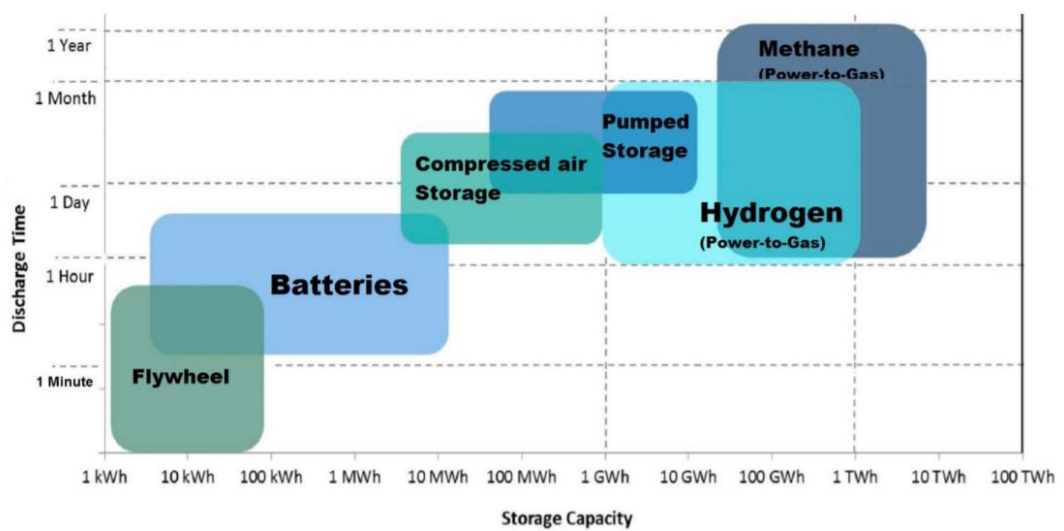


Figure 1.2: Different Energy storage with their capacity and storage time [4]

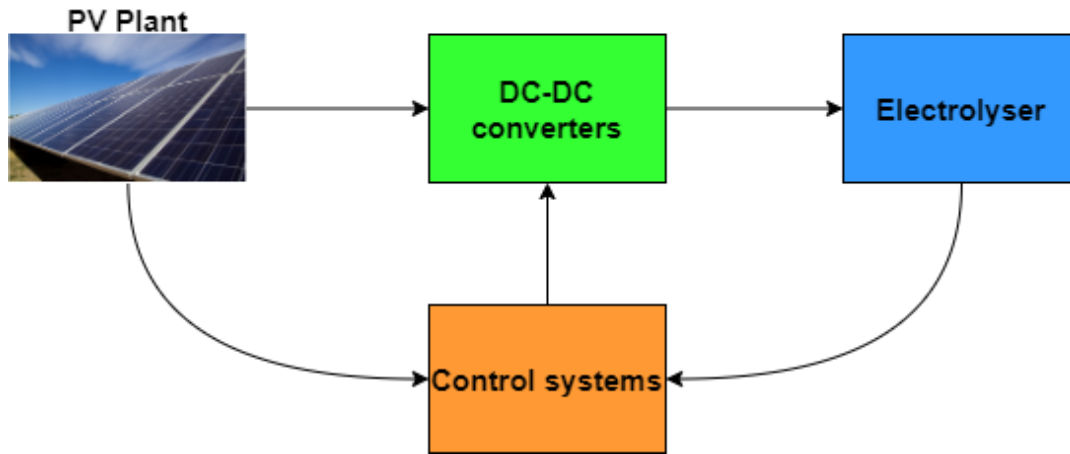


Figure 1.3: PV electrolyser application

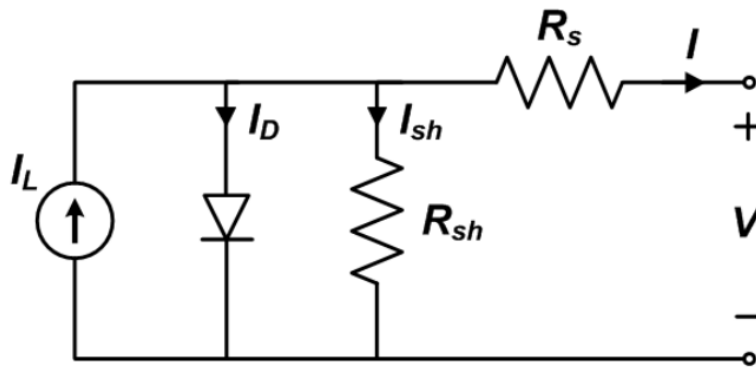


Figure 1.4: one-diode equivalent model solar cell [7]

$$V_T = \frac{kT}{q} \times nI \times N_{cell} \tag{1.2}$$

Making use of the one-diode model and equations 1.1 and 1.2, the following P-V curves Figure 1.5 were generated showing the maximum power point (MPP) for the different irradiance levels. For the PV system used in the model the following parameters were used as shown in Table 1.1.

### 1.3.2. Electrolyser

Hydrogen can be made through the process of electrolysis in which water is split into hydrogen and oxygen atoms as seen in Equation 1.3 . The produced hydrogen can then be used whenever electricity is needed with a fuel cell. The energy needed for the process of making hydrogen through electrolysis can be supplied by different renewable energy sources, for this project solar energy from Photovoltaic (PV) panels was selected.

Table 1.1: PV system parameters SunPower SPR-315E-WHT-D

| Parameters        | Value    |
|-------------------|----------|
| $V_{oc}$          | 64.6 V   |
| $V_{mpp}$         | 54.7 V   |
| $I_{sc}$          | 6.14 A   |
| $I_{mpp}$         | 5.76 A   |
| $P_{mpp}$         | 315.07 W |
| Series x Parallel | 9x2      |

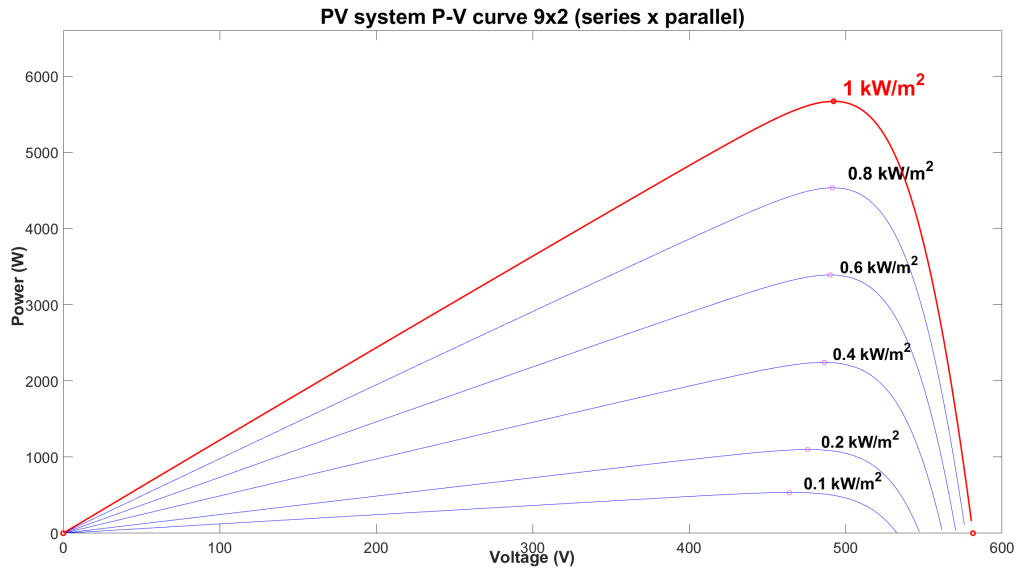


Figure 1.5: P-V curve of the Photovoltaic system

The connection between the PV panels to the electrolyser can be done both directly and indirectly. Both with their respective advantages and disadvantages. Directly connecting the PV panels to the electrolyser has the advantages of having a higher reliability to indirectly connecting the system as there are less components that can cause a failure. Also direct connection can have a better efficiency but only if the PV panels I-V curves are correctly matched to those of the electrolyser but this is only for a certain level of irradiance. The disadvantages include inability to control the power transfer between PV panels and electrolyser and as PV panels maximum power output depends on the weather and cell temperature the efficiency will be lower. Indirect connection allows flexibility in sizing of the system as the power converter would allow attempting to match the I-V curves of the PV panels and electrolyser. Therefore the indirectly connection with a power converter (DC-DC converter) is needed.



### 1.3.3. DC/DC converter

As mentioned above, the connection can be made both directly and indirectly both with their own advantages and disadvantages. In this system the PV system and electrolyser will be connected by usage of power electronics. This will be done with DC-DC converters as both the PV system and the electrolyser are both using a DC(Direct current) connection.

In this PV-electrolyser application there will be 2 converters due to the fact to increase efficiency of the whole system. The first converter will be used for tracking the Maximum Power Point (MPP) of the PV system and will act as an input source to the second converter which connects to the electrolyser. But the control system that has been developed gives the ability to have the PV-electrolyser system to work with one converter only.

For the DC-DC converter at the PV side the following requirements were found

- 1 switch (to reduce the switching losses)
- High efficiency 95-98 %
- High voltage 600 V
- Full tracking range of PV I-V curve
- Power > 5 kW

As for the converter for the electrolyser the following requirements were found [8] [9]

- High voltage conversion ratio 5-10[8]

- Minimal output ripple to improve the electrolyser lifetime [9]
- Minimal cost
- Reliable operation (even after power switch failure) [9]

## 1.4. Research goals

The following research goals/ objectives were selected:

- Find the most suitable DC-DC converters for PV-electrolyser application
  - Literature review of DC-DC converters
  - Simulation of DC-DC converters in Simulink MATLAB
  - Selection of DC-DC converters
- Development of novel control strategy of DC-DC converter for PV-electrolyser application
  - Literature review of control of DC-DC converters
  - Simulation of developed control strategy in Simulink MATLAB

## 1.5. Report outline

To achieve the research goals the report has been divided into several chapters:

- The first chapter: Introduced the idea of the project, the different components & their requirements
- The second chapter: "DC/DC converters" goes into the different converters that can be used for the system and a selection was made after simulations and comparison while taking into account the requirements
- The third chapter: "Electrolyser" presents the different electrolysis methods and which is used and how it is modelled in Simulink Matlab
- The fourth chapter: "Control system" focuses on the different control strategies used in the PV-electrolyzer system and presents the simulation results of the efficiency of the Converter+ algorithm using the developed control strategy.
- The Fifth chapter is the final chapter which presents the conclusions and future recommendations for future research in this area.





# 2

## DC-DC converters

Power electronic converters are power conditioning tools that make use of switches, passive- and active components to control and convert electrical power [10]. As mentioned in The introduction 1 the PV system will be indirectly connected to the electrolyser this will be done by usage of dc-dc converters. These DC-DC converters will be used to track both the maximum power point tracking (MPPT) and supply the electrolyser with the specific voltage level needed for optimal working efficiency.

The DC-DC converter needed for the interconnection between the PV panels and the electrolyzer to produce the hydrogen can be separated into two classes: non-isolated DC-DC converters and isolated DC-DC converters. Due to the electrolyzer having a much lower voltage in comparison to PV panels [9], although some have used boost converters depending on the configuration of the cell voltages of both the electrolyser and PV system [11]. Therefore requiring a step down converter. Figure 2.1 shows the different converters found in literature that will be simulated. The classical converters were used such as buck-boost converter in this PV-electrolyser system [12, 13]. Buck converter was also a good option applied by several researchers, as mentioned before the electrolyser voltage is usually achieved from a step down converter from the PV system voltage [13–15]. Other variations of the Buck converter such as the interleaved buck converter have also been implemented because of its increased reliability and ability to keep functioning after a power electronic switch failure [8].

Isolated converters were also used as they can have higher frequencies due to the transformer. This is to obtain galvanic isolation and can have very high step-down ratios depending on the turn ratio of the transformer [9]. These include half-bridge, full bridge [16, 17] and push-pull [18, 19]. Different variations of stepdown converters such as buck converter and synchronous buck converter (diode replaced by switch to increase the efficiency) were discussed [9]. Several other papers have implemented soft switching converters into their PV-electrolyser systems this is to increase the efficiency of the converter [6, 20, 21]. Soft switching is the idea to have the switching open and close on the 0 point of the voltage or current, this eliminates turn off or turn on losses. But due to this being out of the scope of this project this will be a future recommendation.

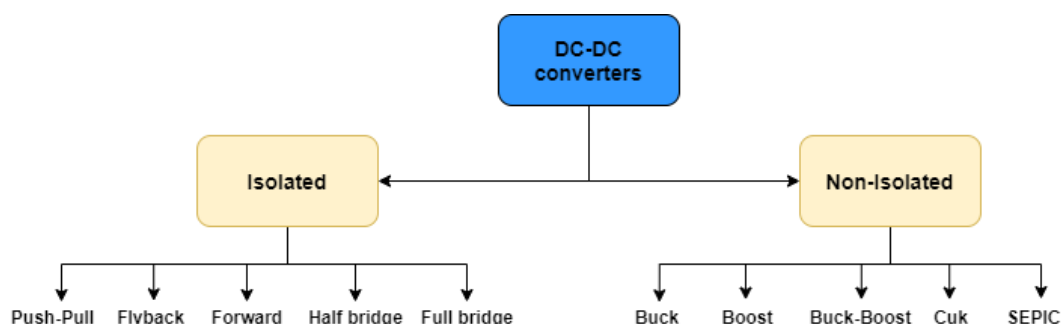


Figure 2.1: Different dc-dc converter configurations isolated vs non-isolated

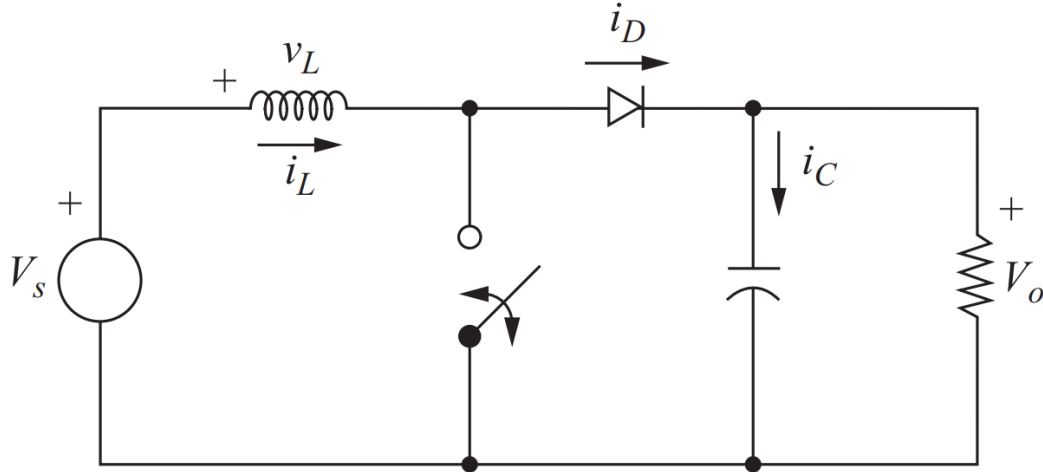


Figure 2.2: Boost converter circuit [22]

## 2.1. Non-isolated DC-DC converters

Non-isolated dc-dc converters include the classical Buck, Boost & Buck-Boost. These converter has the advantage of being simple and of low cost, but having high current and voltage ripples [9]. These ripples can be minimized by increasing the inductor and capacitor value and therefore increases the cost and size of the converter [9]. Also, the switching frequency can be increased to reduce the passive components their sizes but increasing the switching frequency increases both the switching losses and the inductor core losses [9]. Several options are available to improve on the classical buck converter such as replacing the diode with a switch to decrease the losses caused by the diode [9].

### 2.1.1. Boost converter

The boost converter which we can see in Figure 2.2 as the name implies boost the voltage from a lower value to the value that is desired. This is done by periodically opening and closing the switch in the converter [22]. To reduce voltage and current ripples at the output, filters are places at the end .

$$V_{out} = \frac{V_s}{1 - D} \quad (2.1)$$

Equation 2.1 gives the voltage conversion ratio with D the duty cycle. The value of the output current and voltage are calculated with Equations : 2.2 and 2.3

$$\Delta I_L = \frac{DV_s}{Lf_s} \quad (2.2)$$

With the output inductor L value in Henry(H) and  $f_s$  the switching frequency in Hertz (Hz) and the output capacitor C in Farad (F).

$$\Delta V_o = \frac{DV_o}{RCf_s} \quad (2.3)$$

Also the input resistance ( $R_{in}$ ) and output resistance ( $R_o$ ) can be calculated with  $V_{in}$  and  $I_{in}$  known for the system.  $R_{in}$  will vary due to the fact as the duty cycle changes from 0 to 1 depending on required output voltage. The advantages the Boost converter has are the low cost & high efficiency, but one of the disadvantages is that whenever the the load resistance is smaller than the MPP resistance point ( $R_L < R_{MPP}$ ) the MPPT stops working resulting in a non-capture zone [23–25]. This can be seen in figure 2.3

### 2.1.2. Buck converter

Figure 2.4 shows the buck converter circuit with the different components. Buck converter or stepdown converter is used when a lower voltage is needed from the supply voltage. This converter is used often in Electrolyser systems as mentioned before, the electrolyser has a much lower voltage than the source in this case the

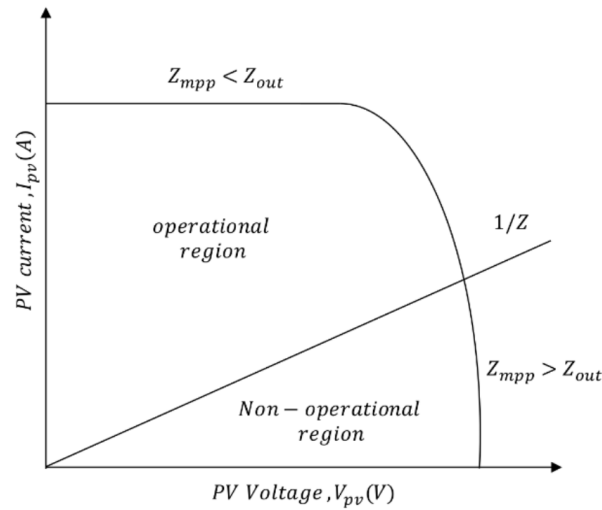


Figure 2.3: Boost converter non-capture zone PV IV curve [25]

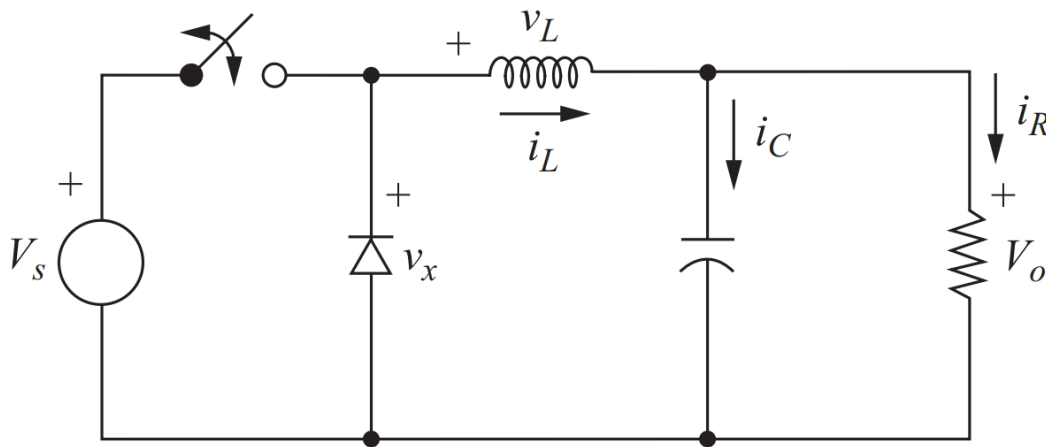


Figure 2.4: Buck converter circuit [22]

PV and also because of the simplicity and low cost [9]. Equations 2.5 and 2.6 show the formulas to calculate the output ripples, from these it can be seen that to keep the inductor size and value small the output ripple will have a high value or the switching frequency can be increase but this would increase the switching losses in the power switch seen in Figure 2.4. But increasing this inductor value will increase the cost and size of the converter [9].

$$V_{out} = V_{in} * D \tag{2.4}$$

$$\Delta I_L = \frac{(1 - D)V_o}{Lf_s} \tag{2.5}$$

$$\Delta V_o = \frac{(1 - D)V_o}{8LCf_s} \tag{2.6}$$

One of the disadvantages is that whenever the the load resistance is bigger than the MPP resistance point ( $R_L > R_{MPP}$ ) the MPPT stops working resulting in a non-capture zone [23–25]. This can be seen in Figure 2.5.

### 2.1.3. Buck-Boost converter

Buck-boost converter is also one of the classical converters which has the ability to either boost or buck the input voltage to the required output voltage by varying the duty cycle. The advantage of this converter is that this converter is a combination of both the buck and the boost converter. This results in this converter having

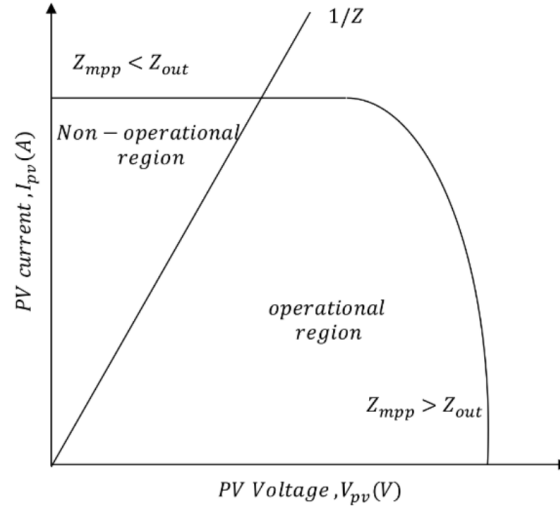


Figure 2.5: Buck converter non-capture zone PV IV curve [25]

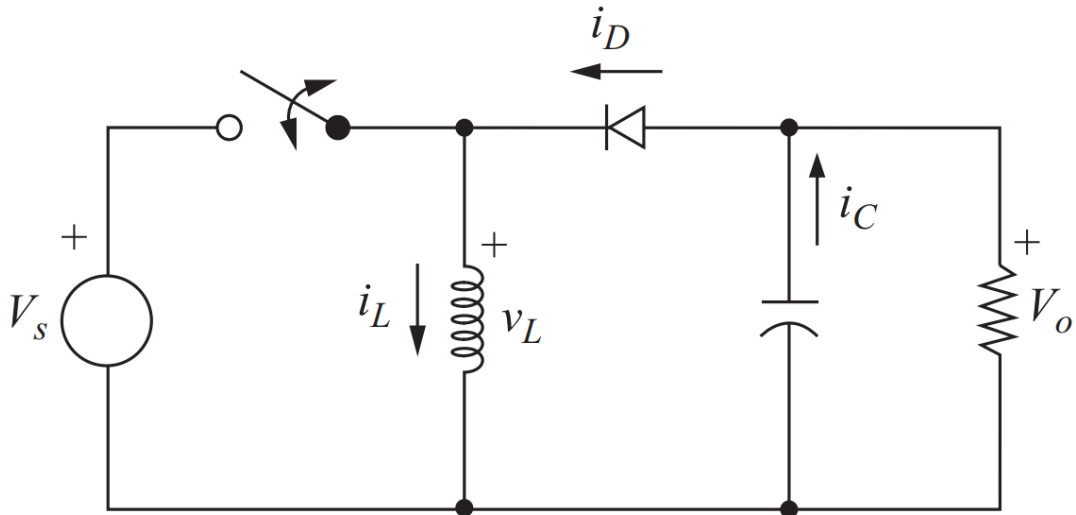


Figure 2.6: Buck-Boost converter circuit [22]

the ability to have full MPP tracking regardless of the load resistance in comparison to the buck converter and boost converter [23–25]. The capture zone of the buck-boost converter can be seen in Figure 2.7, the buck-boost converter has full a full capture zone because it puts together both the buck and the boost converter and overcomes the shortcomings of them as it makes use of both. But the buck-boost converter has an inverted output meaning the output voltage has a different polarity than the input as shown in equation 2.7.

$$V_{out} = -V_s \frac{D}{1-D} \quad (2.7)$$

$$\Delta I_L = \frac{DV_s}{Lf_s} \quad (2.8)$$

$$\Delta V_o = \frac{DV_o}{RCf_s} \quad (2.9)$$

#### 2.1.4. Cuk converter

The cuk converter is just like the buck-boost converter regarding that it can also buck or boost the required voltage and there is also a voltage polarity difference like for the buck-boost converter. The output voltage

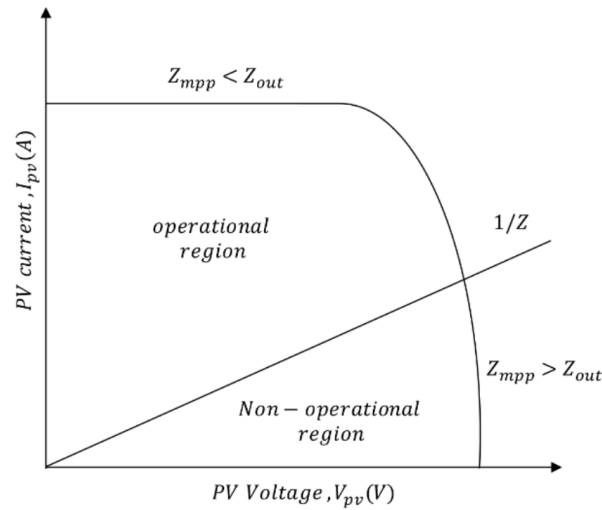


Figure 2.7: Buck-Boost converter capture zone PV IV curve [25]

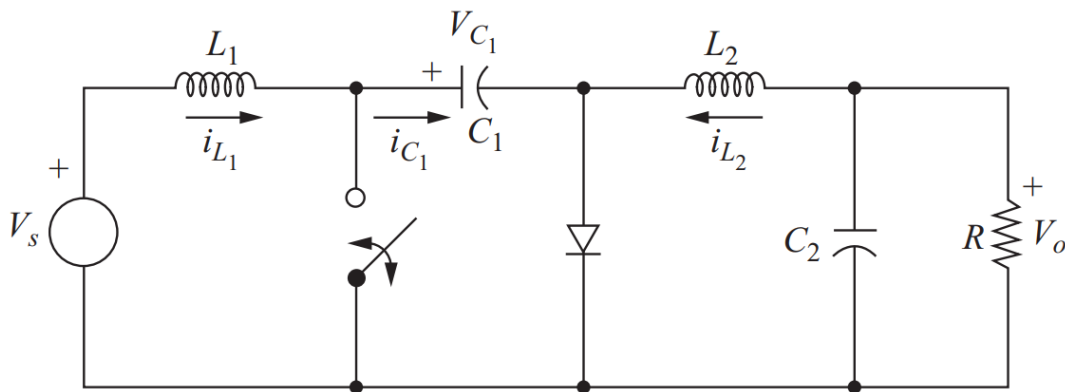


Figure 2.8: Cuk converter circuit

is a different polarity than the input voltage as seen in Equation 2.10. The cuk converter also has the same advantages as the buckboost converter as it has a full tracking range of the PV I-V curve [23–25]. This converter has an extra inductor at the input to filter out harmonics. The other difference between the cuk and the buck-boost converter is that the energy transfer happens in the capacitor C1 instead of the inductor as seen in Figure 2.8. This capacitor is usually also very large and results in the system being ripple free when designed like that. Equations 2.11, 2.12, 2.13 and 2.14 are used to calculate the ripple and the component sizes for this converter. Another difference between the cuk and classical buck-boost is that this converter has 2 more active components which increase cost and size of the converter.

$$V_{out} = -V_s \frac{D}{1 - D} \tag{2.10}$$

$$\Delta V_o = \frac{(1 - D)V_o}{8L_2C_2f_s^2} \tag{2.11}$$

$$\Delta V_{C1} = \frac{DV_o}{RC_1f_s} \tag{2.12}$$

$$\Delta I_{L1} = \frac{DV_s}{L_1f_s} \tag{2.13}$$

$$\Delta I_{L2} = \frac{DV_s}{L_1f_s} \tag{2.14}$$

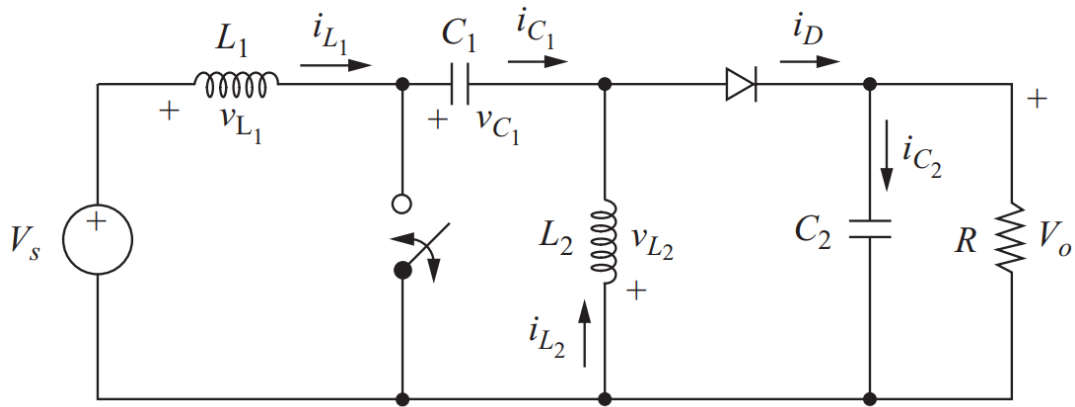


Figure 2.9: SEPIC converter circuit [22]

### 2.1.5. Sepic converter

The Single-Ended Primary Inductance Converter or SEPIC just like the Cuk converter is similar to the buck-boost converter but it does not have the polarity reversal like the other two converters (buck-boost and cuk) as seen in equation 2.15. SEPIC converter transfers all its energy via the series capacitor, due to this a capacitor with high capacitance and current handling capability is required [22]. Other advantages the SEPIC converter has just like the buck-boost converter and cuk converter is that they all have full tracking range of the PV I-V curve [23–25].

SEPIC converter also has 2 extra components just like cuk converter, increasing the cost and size of the converter

$$V_{out} = V_s \frac{D}{1-D} \quad (2.15)$$

$$\Delta V_o = V_{C2} = \frac{DV_o}{RC_2 f_s} \quad (2.16)$$

$$\Delta V_{C1} = \frac{DV_o}{RC_1 f_s} \quad (2.17)$$

$$\Delta I_{L1} = \frac{DV_s}{L_1 f_s} \quad (2.18)$$

$$\Delta I_{L2} = \frac{DV_s}{L_2 f_s} \quad (2.19)$$

### 2.1.6. Interleaved Buck Converter

From the buck converter, interleaved buck converters have been developed. Interleaved or multiphasing buck converters are multiple buck converters connected in parallel. This increases the amount of transferable power in the system [9]. The amount of parallel connections can be from 2 to 6 [9]. The Pulse Width Modulation (PWM) signals (controlling signals) of the duty cycle to the power switches in the converter are all shifted from each other by the amount of parallel connections ( $360/n$ ) [9] [22]. Regarding the overall converter configuration taking into account the components volume, output voltage & current ripples and energy efficiency optimization, 3-leg interleaved buck converter is shown to be the best configuration [9].

$$V_{out} = V_{in} \cdot D \quad (2.20)$$

$$\Delta I_L = \frac{D(V_s - V_o)}{L2 f_s} \quad (2.21)$$

With formula 2.21 the output current ripple can be calculated and also the inductor value can be calculated for a given current ripple that is wanted [26]. This inductor value is the total inductor value in Henry (H) and should be divided by the number of parallel connections in the converter circuit [26].

$$\Delta V_o = \frac{(1-2D)V_o}{8LC(2f_s)^2} \quad (2.22)$$

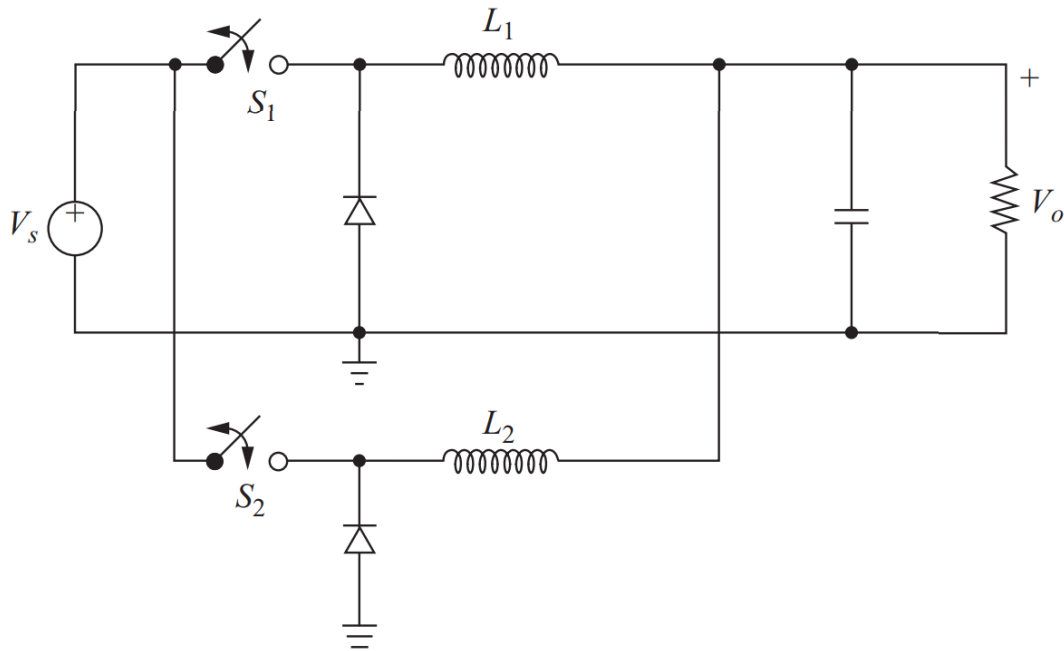


Figure 2.10: Interleaved Buck Converter circuit [22]

## 2.2. Isolated DC-DC converters

The isolated converters as the name implies give isolation from the input to output by using a transformer in between. This also give the flexibility of having boosting and bucking features depending on the turn ratio of the transformer. Although the isolation is not absolute as a too high voltage can break the insulation and result in a current flow [27]. Other advantages of isolated DC-DC converters are breaking of ground loops, this means that the input and output have different ground connections, resulting in that noise can be separated which causes interference [28].

### 2.2.1. Flyback converter

The flyback converter is a isolated converter capable of making the voltage higher or lower depending on the turn ratio of the transformer and dutycycle. The circuit diagram is shown in Figure 2.11. The working principle of this converter is that when the switch is closed the supply voltage is connected to the primary side of the transformer and the current increases in this transformer storing energy in there, the voltage induced at the secondary side is negative during this time period resulting in the diode to block (reverse biased) and the output capacitor supplies the load of its energy. In the time period that the power electronic switch is open, the current on the primary side reduces and the voltage at the secondary side is positive resulting in the diode being forward biased which means that current can flow from the transformer. This energy coming from the transformer supplies the load of energy and also recharges the output capacitor. The disadvantage from using a flyback is that this converter is conventionally used in smaller applications in lower power requirements around 1 kW [29]. Flyback Converter Equations 2.23, 2.24 and 2.25 are used to calculate the component sizes and ripple of the output voltage and current with  $L_m$  being the magnetizing inductance of the primary side of the transformer in Henry(H).

$$V_{out} = V_s \frac{D}{1-D} \frac{N_2}{N_1} \quad (2.23)$$

$$\Delta I_{Lm} = \frac{DV_s}{Lf_s} \quad (2.24)$$

$$\Delta V_o = \frac{DV_o}{RCf_s} \quad (2.25)$$

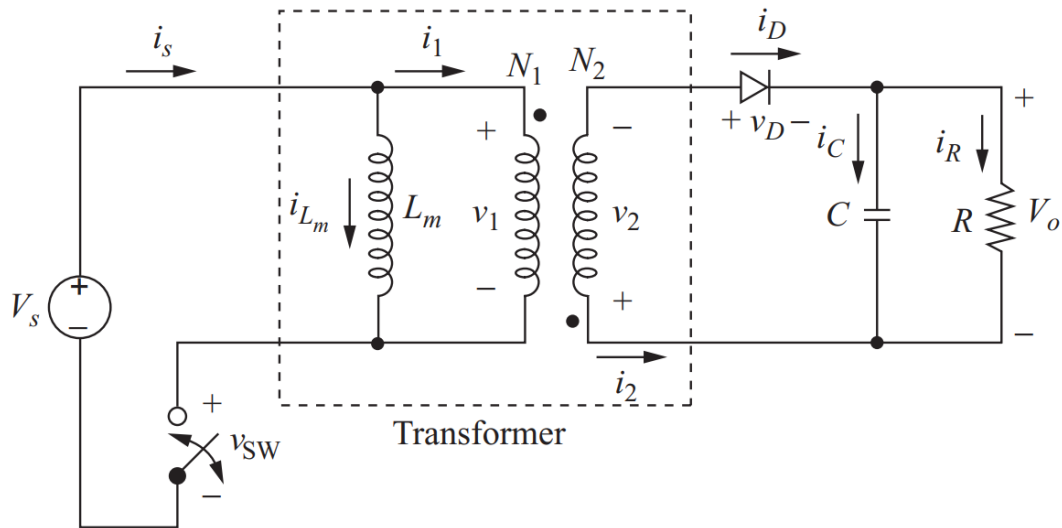


Figure 2.11: Flyback converter circuit [22]

### 2.2.2. Forward converter

The forward converter is another isolated converter using a transformer. But this converter has 3 windings the first 2 windings are used to transfer power from the input to the output and the third winding is used to reduce the magnetizing current when the switch is open to zero at the start of each switching period. For the forward converter the energy is transferred from input to output when the switch is closed but for the flyback this was different as the energy is stored in  $L_m$  first and transferred to the load when the switch is open. The inductor  $L_m$  in the forward converter is not used for the input to output relations, but for demagnetize the transformer and is conventionally made large [22] [27]. Forward Converter components are computed with Equations 2.26, 2.27, 2.28 and 2.29. With  $L_m$  the magnetizing inductance and  $L_x$  the output inductor both in Henry(H).

$$V_{out} = V_s D \frac{N_2}{N_1} \quad (2.26)$$

$$\Delta I_{L_x} = \frac{(1-D)V_0}{L_x f_s} \quad (2.27)$$

$$\Delta I_{L_m} = \frac{D V_s}{L f_s} \quad (2.28)$$

$$\Delta V_o = \frac{D V_o}{R C f_s} \quad (2.29)$$

### 2.2.3. Push-Pull converter

The push-pull converter is another converter that has the ability to either boost or buck the voltage. The name implies the feeding (pushing) of the current and pulling of the current in different switching periods from the transformer [22] [29]. This is done by the two switches seen in Figure 2.13 which give pulses of opposite polarities to the windings of the transformer. The diodes at the secondary side rectify the waveform producing the required DC voltage. The following Equations 2.30, 2.31 and 2.32 are used to calculate the component sizes and output ripples.

$$V_{out} = 2 V_s D \frac{N_s}{N_p} \quad (2.30)$$

$$\Delta I_{L_x} = \frac{D(V_s \frac{N_s}{N_p} - V_o)}{L_x f_s} \quad (2.31)$$

$$\Delta V_o = \frac{V_o(1-2D)}{32 L_x C f_s^2} \quad (2.32)$$



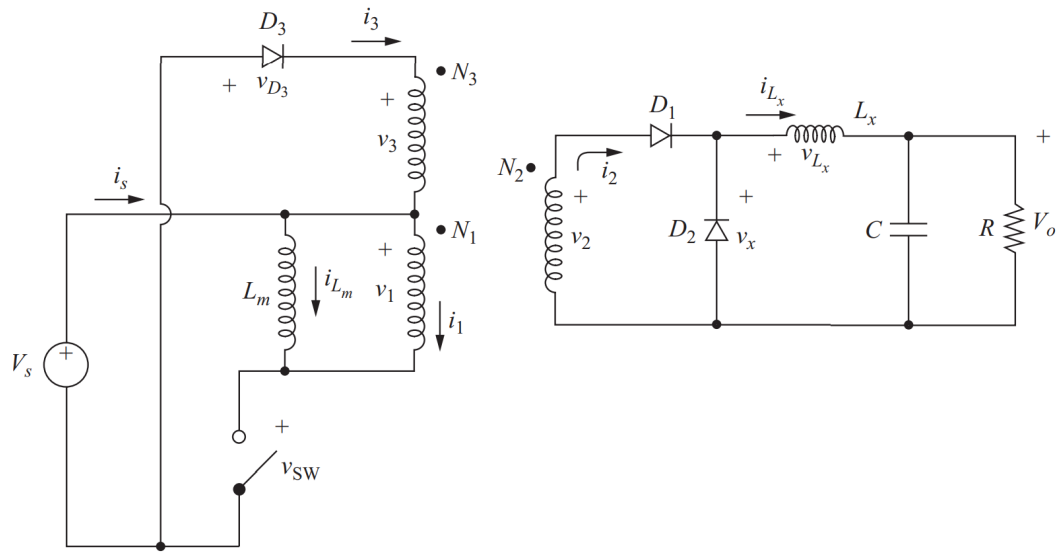


Figure 2.12: Forward converter circuit [22]

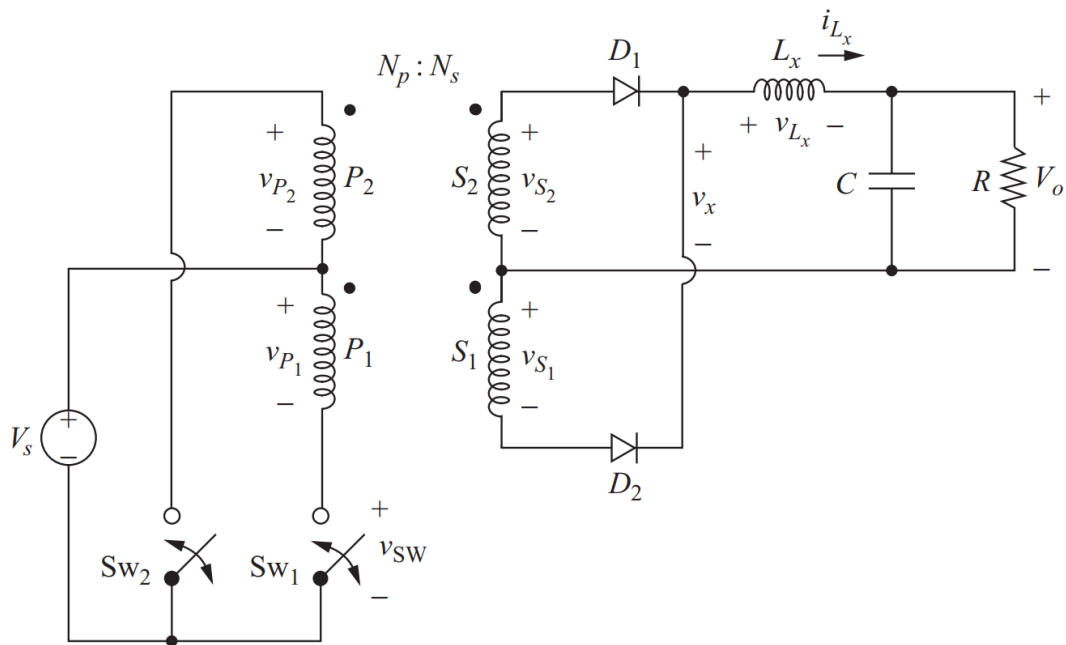


Figure 2.13: Push-Pull converter circuit [22]

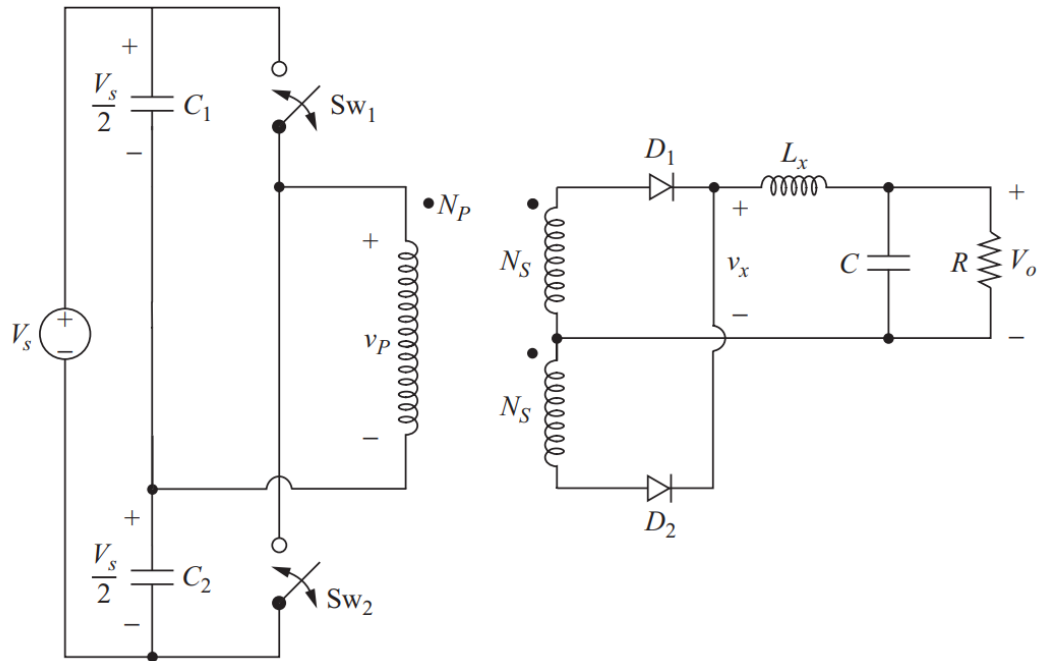


Figure 2.14: Half-Bridge converter circuit

### 2.2.4. Half-Bridge converter

The half-bridge converter is similar to the push-pull converter in operation, the voltages have the same form but for the half bridge the amplitude is half of the value of the push-pull and full-bridge converter [22] [27]. This can also be seen in Equation: 2.33. Due to the fact that the input capacitors (which are equal in size) split the voltage in half resulting in half the input voltage being applied over the transformer [22] which can be seen in Figure 2.14. The following Equations 2.33 2.34 2.35 are used to calculate the component sizes and output ripples. With  $N$  being the turn ratio of the transformer primary and secondary side respectively,  $L_x$  the inductor at the output in Henry (H) and the output capacitor  $C$  in Farad (F).

$$V_{out} = V_s D \frac{N_s}{N_p} \quad (2.33)$$

$$\Delta I_{Lx} = \frac{D(V_s \frac{N_s}{N_p} - V_o)}{L_x f_s} \quad (2.34)$$

$$\Delta V_o = \frac{V_o(1-2D)}{32L_x C f_s^2} \quad (2.35)$$

### 2.2.5. Full-Bridge converter

The full bridge converter is also similar to the push-pull converter as the same voltage is over the transformer. When switch 1 and 2 are closed as seen in figure 2.15 the voltage is  $V_s$  over the primary side. And when switch 3 and 4 are closed this voltage becomes  $-V_s$  [22] [27]. Another difference between these two converters is that the switch rating or the maximum voltage the switch should be able to block is  $V_s$  in the full bridge case instead of  $2V_s$  [22]. The following Equations 2.36, 2.37 and 2.38 are used to calculate the component sizes and output ripples. With  $N$  being the turn ratio of the transformer primary and secondary side respectively,  $L_x$  the inductor at the output in Henry(H) and the output capacitor  $C$  in Farad (F).

$$V_{out} = 2V_s D \frac{N_s}{N_p} \quad (2.36)$$

$$\Delta I_{Lx} = \frac{D(V_s \frac{N_s}{N_p} - V_o)}{L_x f_s} \quad (2.37)$$

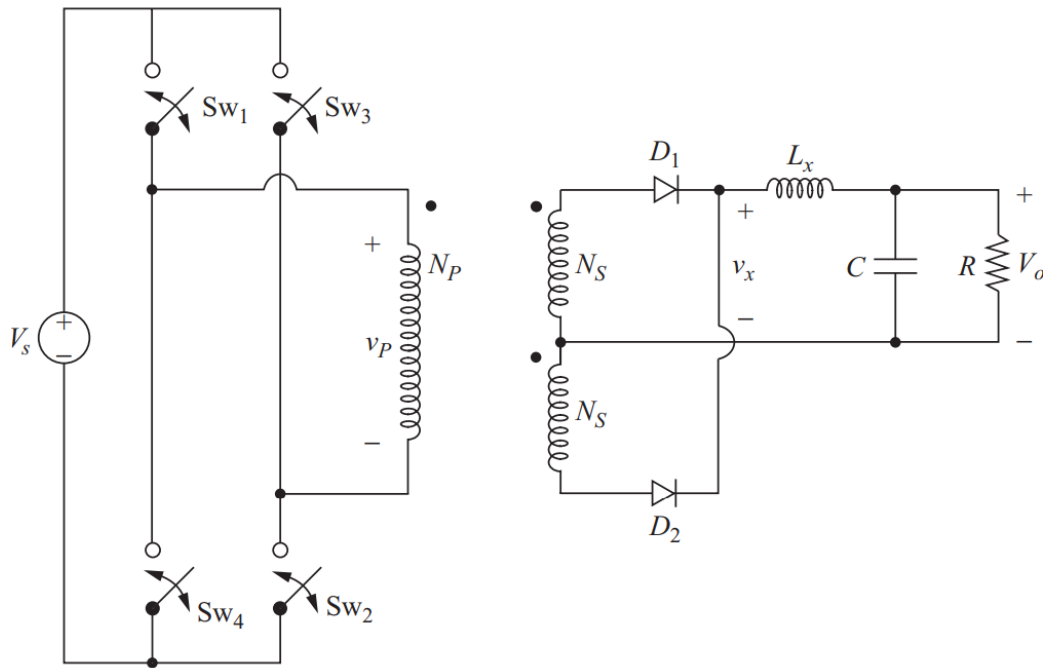


Figure 2.15: Full-Bridge converter circuit

$$\Delta V_o = \frac{V_o(1-2D)}{32L_x C f_s^2} \quad (2.38)$$

Table 2.1: Simulation parameters

| Parameters                            | Value                         |
|---------------------------------------|-------------------------------|
| PV Power(1000 – 500W/m <sup>2</sup> ) | 5000W at 1000W/m <sup>2</sup> |
| Switching frequency                   | 1000 Hz                       |
| Desired $\Delta V_o$                  | 0.01                          |
| Desired $\Delta I_o$                  | 0.01                          |
| Vs                                    | 614                           |
| Turn ratio(n)                         | 1/3                           |

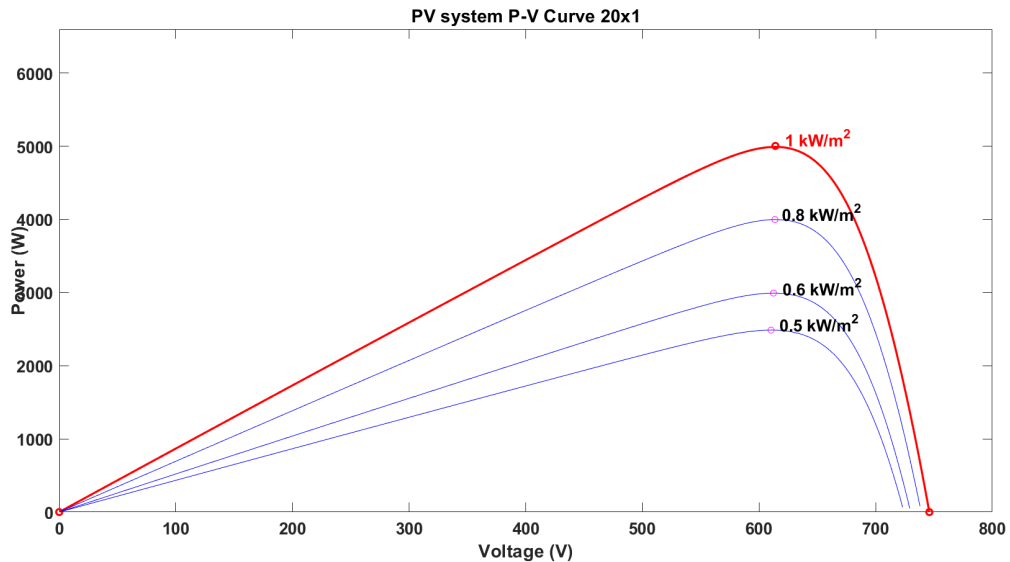


Figure 2.16: Simulated PV system

### 2.3. SIMULINK results & comparison

After doing the literature review for the different dc-dc converters, these converters were modelled and simulated in MATLAB Simulink, while also making use of the found formulas above. All converters were modelled with a Maximum power point tracking (MPPT) controller and the ripples and component sizes were compared.

The component sizes were calculated using the the shown formulas in the past subsections. The following parameters were used for the PV system as seen in table 2.1. The PV system selected for this simulation was 5000 W in size and irradiance levels of 500,600,800,1000 W/m<sup>2</sup> The other parameters selected for the simulation and calculation of the component sizes can be seen in Table 2.1. The PV system PV and IV curve can be seen in Figure 2.16

Figure 2.17 shows the Buck-Boost converter simulated in Simulink MATLAB. The IGBT switch is controlled by the MPPT controller. More on this MPPT controller will be explained in Chapter 4. The PV system is connected to the Converter with a input capacitor in parallel. This capacitor is to filter out any noise and ensures a dc voltage with minimum ripple at the input side. At the output a load is connected to see the voltage, current and the ripples of the system for the given parameters 2.1.

Figures 2.18 2.19 2.20 show the simulation results from the Buck-boost converter Figure 2.18 shows the MPPT power extracted from the PV side with the different irradiance during the simulated time. At irradiance level 1000W/m<sup>2</sup> the output power is 5000W showing that the MPPT is working when compared to Figure 2.16 which shows the P-V curve of the PV system for the different irradiance levels.

Figure 2.22 and 2.23 show the output Power, voltage and current coming from the Interleaved Buck converter. These plots were used to calculate the output ripples of the Interleaved Buck converter. The zoom in on Figure 2.23 is zoomed in at the time period when the irradiance is 500W/m<sup>2</sup>.

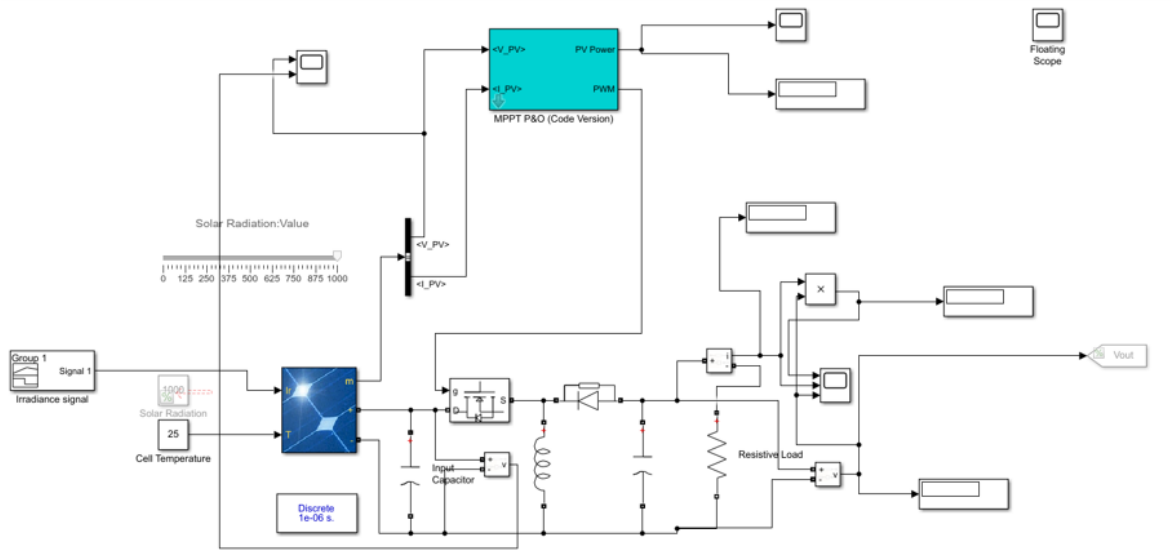


Figure 2.17: Buck-Boost converter in SIMULINK with MPPT controller

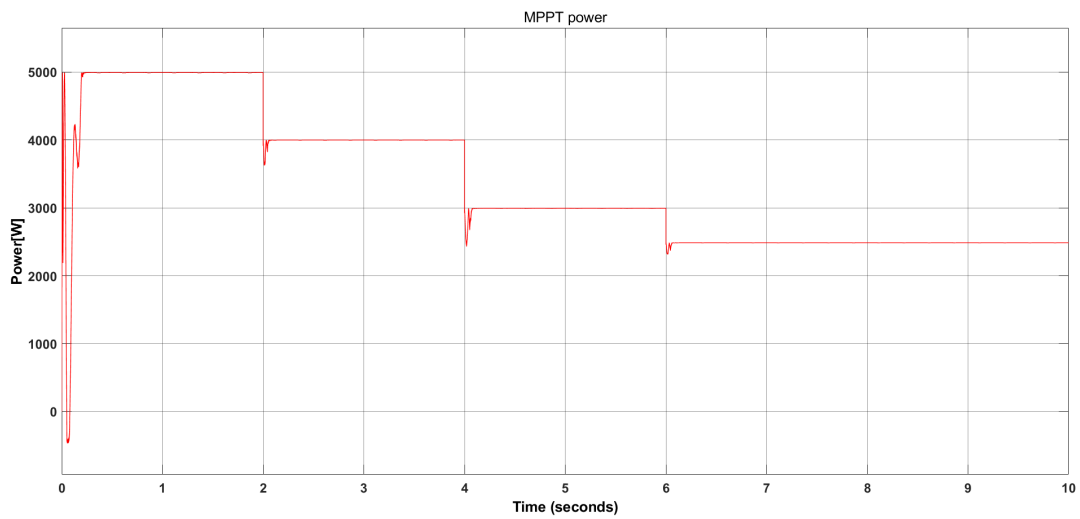


Figure 2.18: PV MPPT power buckboost converter

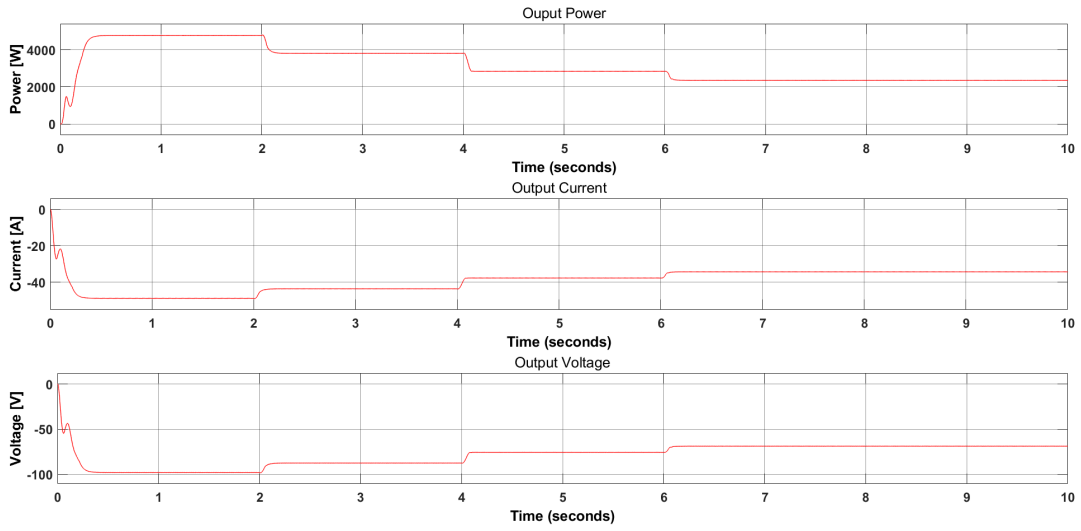


Figure 2.19: Buck-Boost converter output Power, Current & Voltage

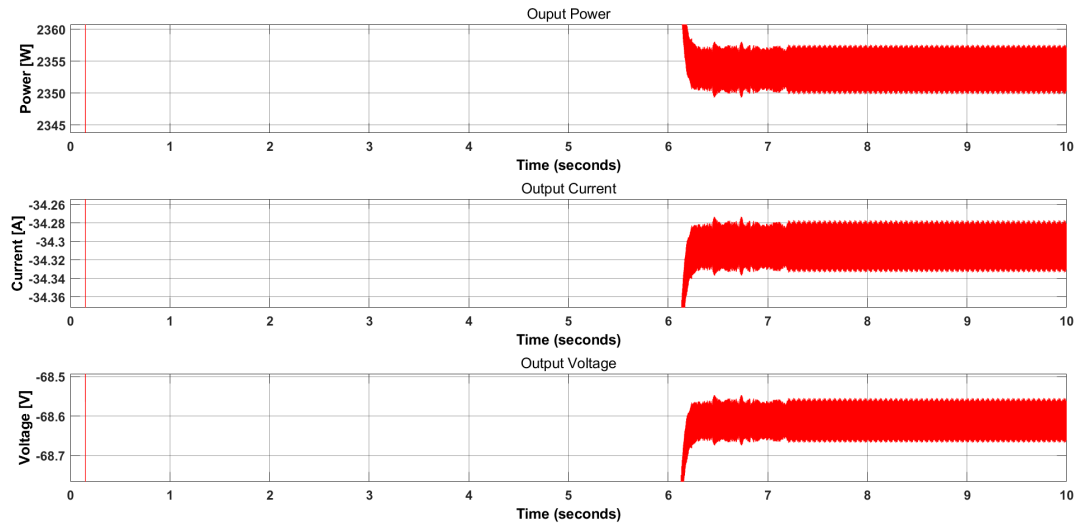


Figure 2.20: Buck-Boost converter output Power, Current & Voltage Zoomed in

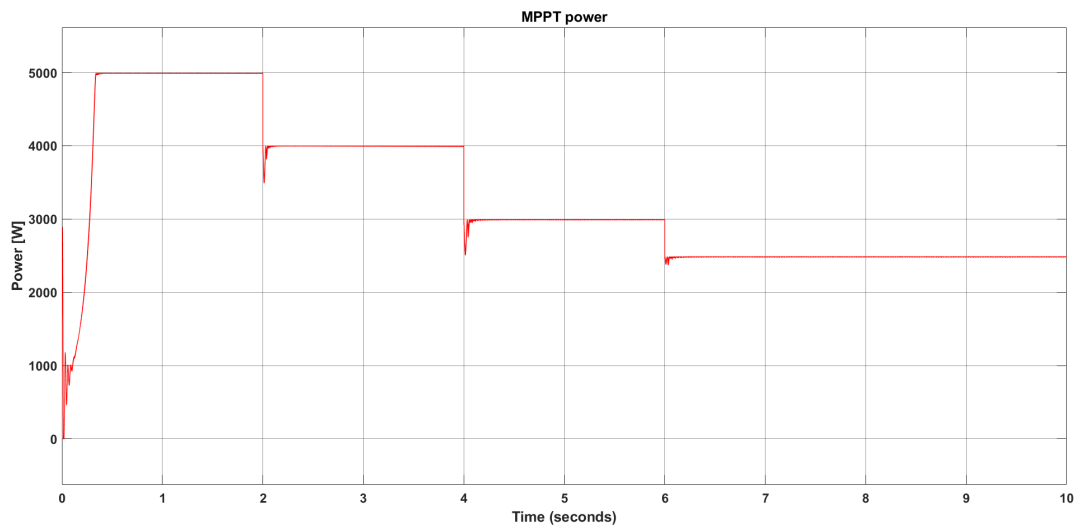


Figure 2.21: PV MPPT power Interleaved converter

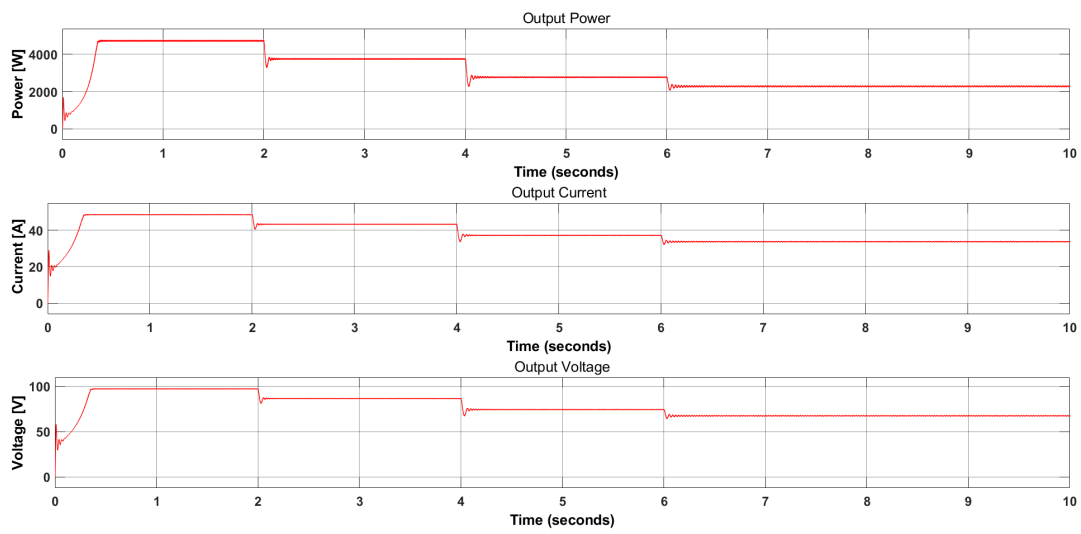


Figure 2.22: Interleaved converter output Power, Current & Voltage

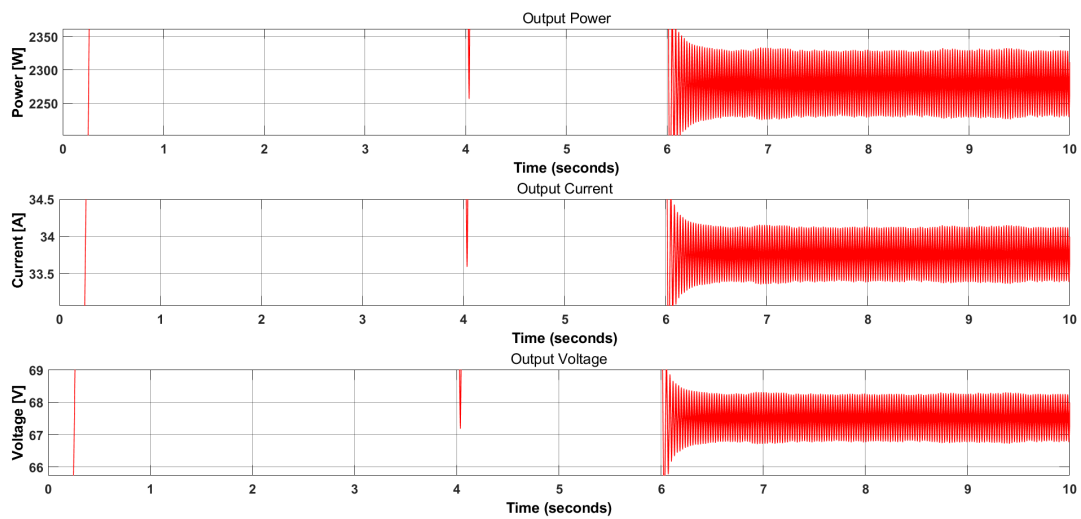


Figure 2.23: Interleaved converter output Power, Current & Voltage Zoomed in

Table 2.2: Converter Parameters

|                       | Buck     | Boost    | Buck-Boost | Cuk      | SEPIC    | Push-pull | Forward  | Flyback  | Interleaved | Half-bridge | Full-bridge |
|-----------------------|----------|----------|------------|----------|----------|-----------|----------|----------|-------------|-------------|-------------|
| Peak input power [W]  | 5000     | 5000     | 5000       | 5000     | 4990     | 4991      | 4990     | 4990     | 4991        | 4991        | 4991        |
| Peak output power [W] | 4825     | 4850     | 4825       | 4900     | 4940     | 4880      | 4350     | 4655     | 4780        | 4950        | 4875-4810   |
| Input power ripple    | 4%       | 1%       | 4%         | 0.60%    | 1%       | 0.34%     | 1.50%    | 4%       | 0.50%       | 1%          | 1%          |
| Lo [H]                | 1.80E-01 | 9.00E-03 | 1.60E-01   | 2.00E-03 | 8.60E-03 | 6.00E-02  | 5.00E-02 |          | 1.04E-01    | 2.50E-03    | 6.00E-02    |
| Co [F]                | 6.25E-05 | 3.10E-04 | 5.30E-03   | 1.25E-02 | 7.00E-03 | 3.13E-05  | 1.60E-04 | 3.00E-02 | 7.87E-06    | 3.00E-04    | 3.13E-05    |
| Ls [H]                |          |          |            | 7.80E-03 | 5.30E-03 |           | 4.90E-02 |          |             |             |             |
| Cs [F]                |          |          |            | 2.00E-03 | 2.00E-03 |           |          | 5.50E-05 |             |             |             |
| Voltage ripple        | 0.65%    | 0.57%    | 1.02%      | 3%       | 2.75%    | 0.80%     | 1.00%    | 2.19%    | 2.40%       | 1.72%       | 1.15%       |
| Current ripple        | 0.63%    | 0.57%    | 1.16%      | 3.30%    | 2.75%    | 0.80%     | 1.10%    | 2.12%    | 2.44%       | 1.61%       | 0.75%       |
| Switch rating (Vs)    | Vs       | Vs       | Vs         | Vs       | Vs+Vo    | 2Vs       | 2Vs      | Vs+Vo(n) | Vs          | Vs          | Vs          |
| number of switches    | 1        | 1        | 1          | 1        | 1        | 2         | 1        | 1        | 3           | 2           | 4           |
| number of diodes      | 1        | 1        | 1          | 1        | 1        | 2         | 3        | 1        | 3           | 2           | 2           |



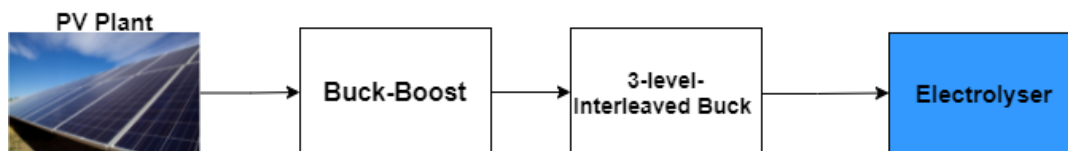


Figure 2.24: Selected converters in PV-electrolyser system

Table 2.1 shows the different parameters which have been calculated and simulated using both the formulas found from literature and simulation done in Simulink. The components were calculated with a matlab script using the formulas shown in the above mentioned sections. In the first row we see the peak input power that is drawn from the pv system with help of the MPPT in this case using a P&O method. As mentioned in Table 2.1 the PV system max power for this simulation was 5000 W at  $1000W/m^2$  irradiance showing that the MPPT controller is working correctly. Row 2 shows the output power at  $1000W/m^2$  irradiance for the different converters most close to 5000 W but depending on the losses less power is achieved at the load of the converter output. The different converter component sizes such as the inductor and capacitor and in some cases the extra inductor and capacitor depending on the converter configuration are also shown. Also included are the Voltage and current ripples found at the output for the simulation which in most cases were found to be close to 1% as used in the formulas in the matlab script.

The last 2 rows show the amount of diodes and switches the different converters use in their configurations such as for the classical converters and cuk and sepic only 1 switch and 1 diode is needed. but the isolated converters with transformers which also increases the costs have 2 switches and 2 diodes at least. The interleaved buck converter in this simulation was a 3 level interleaved buck converter as this is the best configuration for a interleaved buck converter. As this 3 level interleaved buck converter is the optimal configuration in terms of components volume, output current & voltage ripples and the efficiency [9]. Another important component is the switch voltage rating for each converter, this voltage rating is the voltage the switch should be able to block when it is open. This value is different for each converter and can also be found in Table 2.2.

The buck and boost converters have good input and output power range. But they do not have the ability to track the full I-V curve of the PV system for the MPP as shown in Figures 2.5 and 2.3. The Sepic and cuk converters have 2 extra components which increases the size and costs of the system. The buck-boost converter has the full tracking range of the PV system I-V curve and has less components compared to the cuk and sepic converter. The other converters are all isolated converters and have transformers which increase the cost. Taking into account the requirements shown in the Introduction 1 and the above shown results regarding the parameters of the different converters and its ability to fully track the PV IV curve for the MPPT converter the buck-boost converter is chosen. As for the converter chosen for the electrolyser, given the requirements of having the ability to work even after a power electronic switch failure the interleaved buck converter is chosen. The full-bridge converter also has great potential as this has highest voltage ratio of the simulated converters and given that the electrolyser voltage is much lower than a typical PV system this converter is also a great choice if the costs of the transformer is neglected and available. The selected converters can be seen in Figure 2.24 in the PV-electrolyser system.



# 3

## Electrolyser

As mentioned in the Introduction 1 the idea is for this system to produce green hydrogen by using a renewable energy source in this case PhotoVoltaics. The advantages of producing Hydrogen to later produce energy include:

- High electrochemical reactivity [30]
- High energy density [30]
- Unlimited availability (Depending on the amount of water there is) [30]
- Green for the environment (safe combustion after product (water)) [30]

The different systems that perform water electrolysis will be explained in this chapter.

Hydrogen is made through the electrolysis of water, In this chemical reaction water is split into both hydrogen and oxygen. This electrolysis can be done by multiple different types of electrolysers: Alkaline, Proton exchange membrane (PEM) and solid oxide high-temperature electrolysis [30].

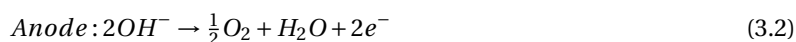
Alkaline electrolysers have been used in [6, 13, 19, 31–34] and the PEM Electrolysers in [8, 11, 12, 14, 21, 35].

### 3.1. Alkaline electrolysis

Alkaline electrolysers have been in the industry for more than 100 years and are cheaper than the PEM electrolysers but have a lower efficiency [36]. Other advantages include low cost, high durability and using non noble catalysts in the system [37]. The working principle of the alkaline electrolyser is that a specific potential voltage 1.2-2 V [30] is applied to the system electrodes as shown in Figure 3.2. At the cathode the following chemical reaction takes place where water is split into oxygen, protons and electrons [38].



The chemical reaction at the cathode is the following: Here the Protons from the anode reaction combine with the electrons resulting in hydrogen gas.



Taking both reactions at the electrodes, this results in a total chemical reaction of:



### 3.2. Proton exchange membrane (PEM) electrolysis

Proton exchange membrane electrolysers were introduced to overcome the disadvantages of the Alkaline [39]. These include overcoming the problem of working in low load situations, low-current and pressure in the alkaline system [39]. Because of the high current density the cost of operation goes down for these systems

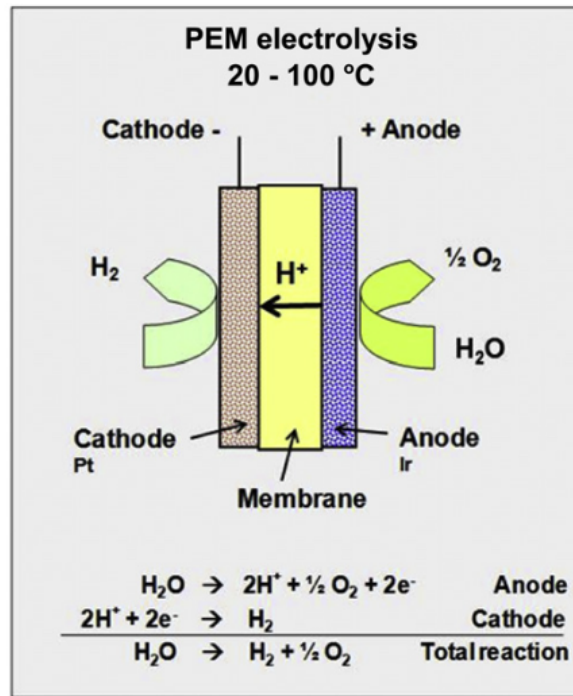


Figure 3.1: PEM Electrolyser diagram [39]

[37]. Figure 3.1 shows the configuration of a PEM electrolyser with the different chemical reactions that take place. Other advantages from the PEM electrolyser are its high purity of hydrogen gas that is produced [37] and its compact design. But because of the use of the membrane the costs of the different components are high [37]. It has not yet been as much applied as the alkaline electrolyser and the power capacity for now is smaller compared to the alkaline electrolyser [37].

### 3.3. Solid oxide high temperature electrolysis

The Solid oxide high temperature electrolysers are less developed in comparison to the Alkaline and PEM [36]. Although they are capable of having higher efficiencies compared to the other two because of the usage of high temperatures (500-800 C) [36] [37]. The solid oxide electrolysers will be one of the most important whenever their durability issues are solved [37]. As of now these electrolysers are only used in lab scale research [37].

### 3.4. Selected electrolyser: Alkaline electrolyser model

For our system an alkali electrolyser model in MATLAB Simulink was selected which we can see in Figure 3.2. In this system a alkaline electrolyser is used in the SIMULINK environment as a electrolyser emulator with a voltage range of 210-260V and temperature of 20-60 degrees as can be seen in figure 3.3. The electrolyser model is modelled as a look up table with the values seen in figure 3.3. The model works by checking the voltage that is applied over it and taking the current value that is assigned to that value and that value flows through the system.

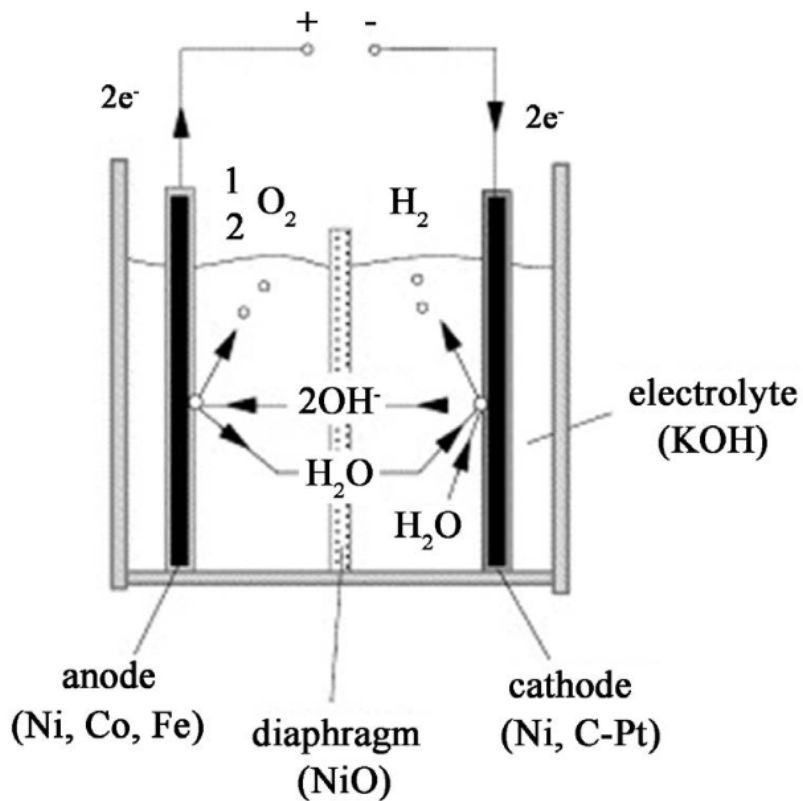


Figure 3.2: Alkaline Electrolyser diagram [40]

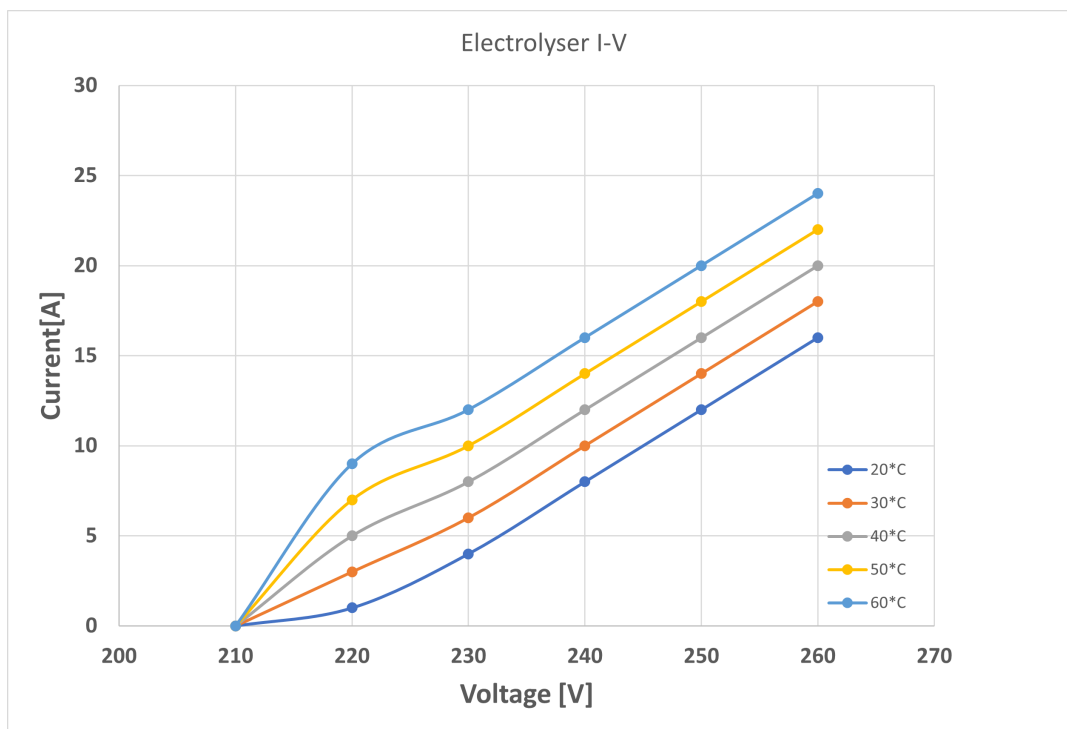


Figure 3.3: V-I curve of the Electrolyser emulator system



# 4

## Control systems

As explained in section 2 in dc/dc converters the output voltage is changed by controlling the duty cycle/PWM signal to the switch and achieving the required value. Controlling this duty cycle will be done by the control system which takes into account the amount of energy that is produced by the PV system, and the amount of energy the electrolyser can use. This is because the I-V curve of the PV system changes with irradiance and the ambient temperature as can be seen in Figure 1.5, also the V-I curve of the water electrolyser emulator changes with temperature as seen in Figure 3.3.

### 4.1. Control algorithms

The system has been developed for both one and two converter models shown in Figures 4.1 and 4.2.

For the two converter model two control strategies have been implemented:

- Maximum power point tracking (MPPT)
- Control algorithm: Power matching

The first control is only used in the model when there are two converters used, the converter that is connected to the PV system in that model uses the MPPT control to find the maximum power point of the PV system. The second control algorithm is for optimizing the working point and efficiency of the whole PV-Electrolyser system, this control strategy can be used in both one converter and two converter models. The following [15][21] uses a current control method to have a constant current flow to the electrolyser, but resulting in losing some of the generated PV power. Other control methods include water heating and water flow control [11] [14]. Ulleberg recommends that the electrolyser should operate in variable power mode instead of fixed to optimize the system [32].

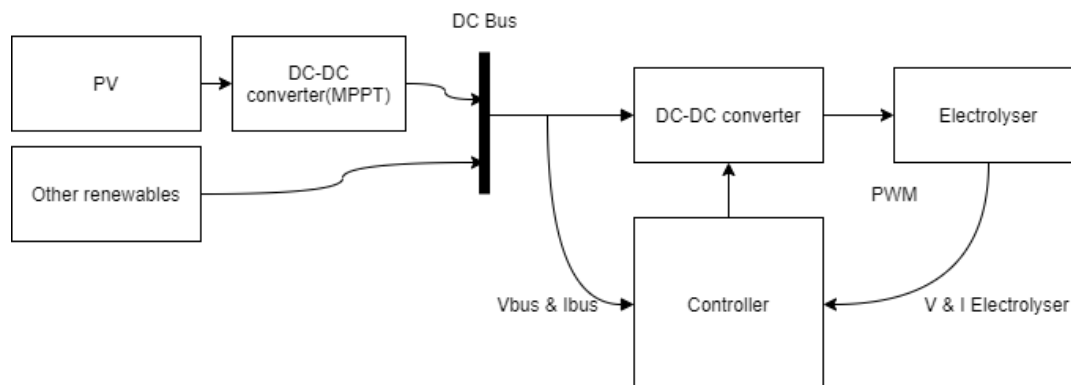


Figure 4.1: PV-electrolyser system with two converters

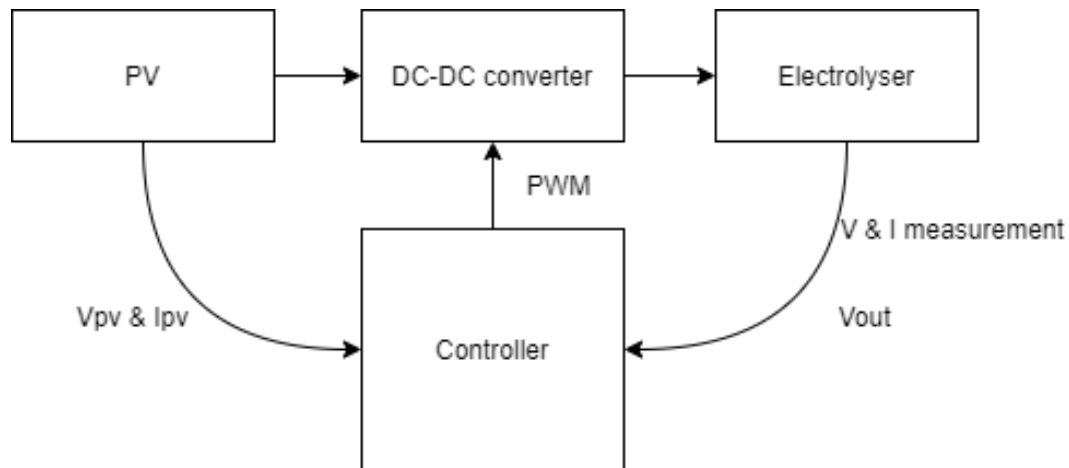


Figure 4.2: PV-electrolyser system with one converter

#### 4.1.1. Maximum power point tracking

The maximum power point tracking (MPPT) will be done only for the two converter model as mentioned in Section 4.1. The MPPT can be done through different algorithms namely :

- Constant voltage method
- Open voltage method
- Short current pulse method
- Perturb & Observe method (P&O)
- Incremental conductance method (IC)
- Temperature methods : Temperature gradient algorithm (TG) & Temperature Parametric equation method (TP)

The first 3 methods are indirect methods as they are mostly hard coded using data and formulas with several corrections and approximations and do not require any measurement signal coming from the PV system [41]. The last 3 methods are direct methods. These methods use Voltage and Current measurements from the PV system to find the actual Maximum power point (MPP).

The constant voltage method uses the specifications of the PV array and applies the voltage that gets the Maximum power point at the specific load, which means a control is needed for variable load conditions [41].

The Open voltage method makes use of the fact that MPP Voltage is a specific fraction of the Open Circuit voltage ( $V_{OC}$ ). The fraction is usually 70-80 % of the open circuit voltage [41].

The Short Current Pulse method uses the same method as the open voltage method but uses current instead of voltage.

The Perturb and Observe (P&O) method makes use of changing the Voltage by a small amount (incremental change) in one direction and seeing how that change influences the power point of the PV system as seen in Figure 4.3. if the power increases the voltage change will keep going in that direction if not the voltage change will be made in the other direction as seen in Figure. P&O method has 3 different methods in itself: 1.the classic which has a constant increment that is used to change the Voltage value, 2.an optimized version but more complex as the value of the perturbation are variable depended on how close it is to the MPP,3. Three points weight comparison P&O .

Perturb and observe is the most commonly used MPPT method in commercial products because of its simplicity,high robustness and and good efficiency [43].

Incremental conductance method calculates the conductance ( $I/V$ ) from the PV voltage and current measurement and also the incremental conductance( $dI/dV$ ) to create a reference voltage ( $V_{ref}$ ) if  $V_{ref}$  is on the left of Maximum power point Voltage( $V_{mpp}$ ) this means the  $dI/dV > I/V$  and if it is on the right of  $V_{mpp}$  , $dI/dV < I/V$  and thus  $V_{ref}$  is increased until the MPP is reached and  $dI/dV = I/V$ .



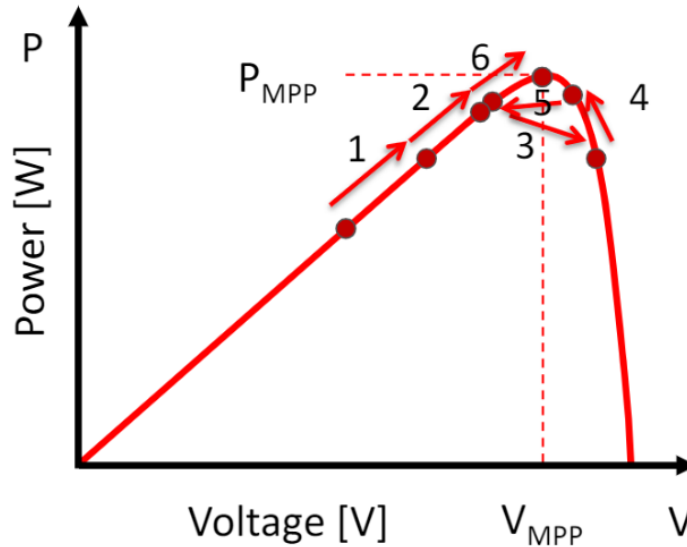


Figure 4.3: Perturb and observe MPPT method [42]

Incremental conductance method is a more complex method as it requires more computation power (as more parameters compared to P&O need to be computed) but has a faster response than the P&O method in varying environmental conditions [41].

There are also temperature methods including the gradient & parametric equation method which measure Irradiance and Temperature to find the VMPP. The gradient method uses an algorithm that checks which Opencircuit voltage matches to the temperature it has just measured and the MPP is found with the open voltage method as mentioned above.

Because of the easy implementation and being most conventional method used the Perturb and Observe method will be used for MPPT.

#### 4.1.2. Control algorithm: Power matching

Because of these changes in temperature and irradiance, the control algorithm will need to take this into account. The control flow chart can be seen in Figure 4.4. This flowchart has the measured values of the voltage and current of both the PV and the electrolyser as its input. After collecting these values the Power is calculated of both the Electrolyser and the PV generator and checked if the power of both sides is matched.

As mentioned in Chapter 3 the voltage range of the electrolyser is 210-260 V and temperature of 20-60 °C. The control of this system is voltage control. With the help of the flowchart the optimal reference voltage is selected to match the Electrolyser power to the PV generated power. The electrolyser in this case is the load and the load point is changed to match the power coming from the PV. If for example the power coming from the PV side is 3000W and the temperature of the electrolyser is 20°C and the starting position of the electrolyser at that time is 230V at point 1 in Figure 4.5 then the algorithm will select the voltage at which this matches the power to 3000 W coming from the PV system, it does this by changing the voltage by a certain delta (stepsize) until it reaches the point where the voltage is 250 V and current 12 A matching the PV power at the electrolyser temperature being 20°C, This algorithm is implemented as Matlab function in SIMULINK. After selecting the reference voltage at 250V this value will go through the voltage controller.

Figure 4.6 shows the complete system diagram with the signals coming and going from each component as we can see for the control algorithm both the Voltage and Current of the Photovoltaic system and from the electrolyser side are needed. As mentioned before, the control algorithm selects a reference voltage. This reference value is compared to the Voltage of the electrolyser and sent into a PI controller after that the signal goes in a PWM generator and the PWM signal to the switch of the converter is generated as shown in Figure 4.6. Also given the inputs the controller uses, this controller can be applied to any dc-dc converter configuration.

Garcia-Valverde did a similar approach to this control. Their algorithm tries to find the optimum and safe operating point for both PV and electrolyser system [12]. The control algorithm can be seen in Figure

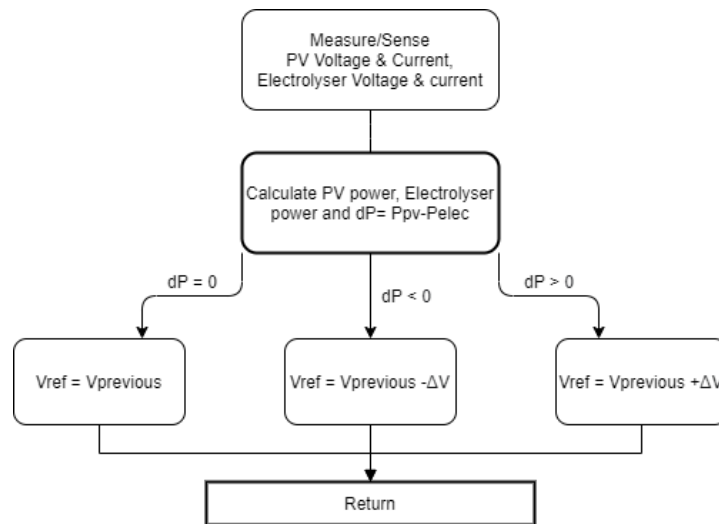


Figure 4.4: Control algorithm flowchart

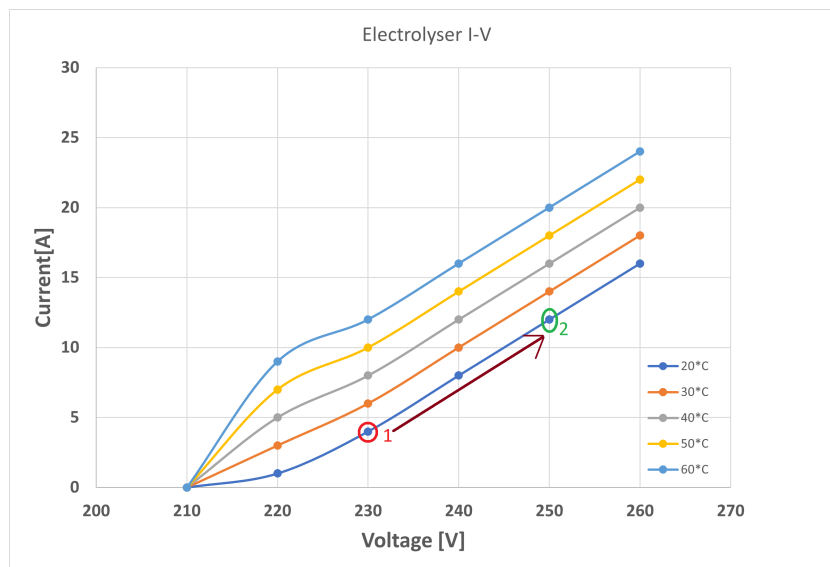


Figure 4.5: Control algorithm power matching

4.7. The algorithm searches for the MPP with an incremental conductance method. While searching for this MPP it is also checked if this MPP is a safe operating point of the system regarding the electrolyser in order to avoid damage to the electrolyser [12]. If the safe operating point is not close to the MPP the control will select the voltage that is closest to the safe operating point. These safe working points of the electrolyser are called the linear interval of the V-I curve. In comparison to the controller built in this report the same inputs are needed for both controllers namely the Voltage and current of both the PV and electrolyser system. The main difference between the controllers would be that in the controller of the paper by Garcia-Valverde the MPP is searched for first with an incremental conductance method, and in the controller in this system the MPP is achieved by changing the load in this case the electrolyser to the right voltage and achieving the MPP. This results in less computation and a simpler controller as there are less steps to take and less values needed to be computed.

## 4.2. Control algorithm SIMULINK simulation

In this section the Control algorithm is simulated in the MATLAB Simulink environment. As mentioned in section 4.1 the system and controller has been built to work in models consisting of one or two converters. For the two converter model, one converter performing the MPP tracking right after the PV system and the

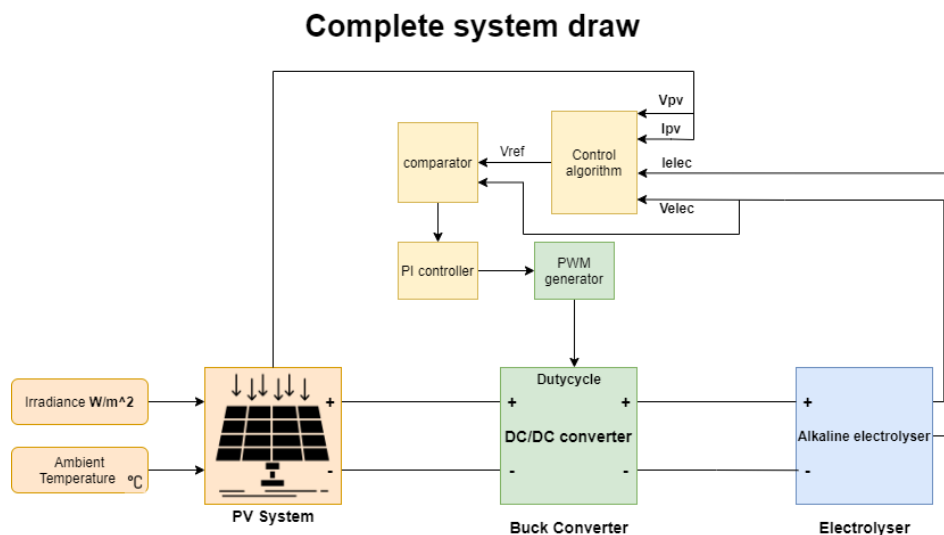


Figure 4.6: Complete system diagram

other converter used to implement the developed controller. And in the one converter model the control algorithm makes sure the maximum power from the PV is extracted and supplied to the electrolyser for the given environmental parameters (irradiance and temperature of both the PV and Electrolyser). In the one converter model the converter that is used is the buck converter. The simulations are done for several different parameters such as changing irradiance but constant electrolyser temperature, changing temperature of the electrolyser but at constant irradiance of the PV system, Varying both the temperature and irradiance of the system. At the end a number of simulations were done for different parameter values of the step size and time delay implemented in the controller to find the efficiency. For these simulation a buck converter was connected to the electrolyser to check the working of the control system as this is the most simple stepdown converter.

#### 4.2.1. Two converter simulation

Figure 4.10 shows the two converter model in the Simulink environment. The PV array with the irradiance and ambient temperature as inputs. The output of the PV system is connected to a boost converter with a MPPT controller this converter ensures the MPPT is tracked and the maximum power from the PV is supplied to the rest of the system. The boost converter is connected to a buck converter that is connected to the electrolyser model. This buck converter its power electronic switch is controlled by the control algorithm explained in section 4.1.2 and ensures the right voltage is delivered to the electrolyser from the buck converter. In this simulation the electrolyser temperature was kept constant at  $20^{\circ}\text{C}$  and at that temperature the highest amount of power the electrolyser can consume is 4160 W as seen in Figure 3.3. In figure 4.9 the simulation result is shown. On top the electrolyser voltage is shown and on the bottom the PV and electrolyser power. In the beginning the irradiance is  $1000\text{W}/\text{m}^2$  and the PV power is around 5600 W, but at  $20^{\circ}\text{C}$  the maximum working load of the electrolyser is 4160 W but after time period four seconds the irradiance drops and the PV power is around 4000 W resulting in the electrolyser working at the point of 4000 W which can be seen also in the voltage going down from 260 V to 258 V on the top part of Figure 4.9. This is the work of the control algorithm selecting the right working voltage for the electrolyser. This continues for the rest of the simulation as the irradiance goes down and the PV power becomes less the electrolyser matches itself to that amount.

#### 4.2.2. Varying Irradiance & constant Temperature

For the next simulations the 1 converter model was used to show that the controller works in both one and two converter models. Figure 4.10 shows the simulated model in MATLAB/Simulink. Just like in the two converter model the PV array has inputs the irradiance and ambient temperature. But in this model the PV array is connected to the input of the buck converter and the output of the buck converter is connected to the electrolyser model. The buck converter power electronic switch is controlled by the control algorithm as explained in Section 4.1.2 to regulate the output voltage. Figure 4.13 a simulation is shown where the electrolyser works at a temperature of  $20^{\circ}\text{C}$  but the irradiance of the PV system changes. On the top of this

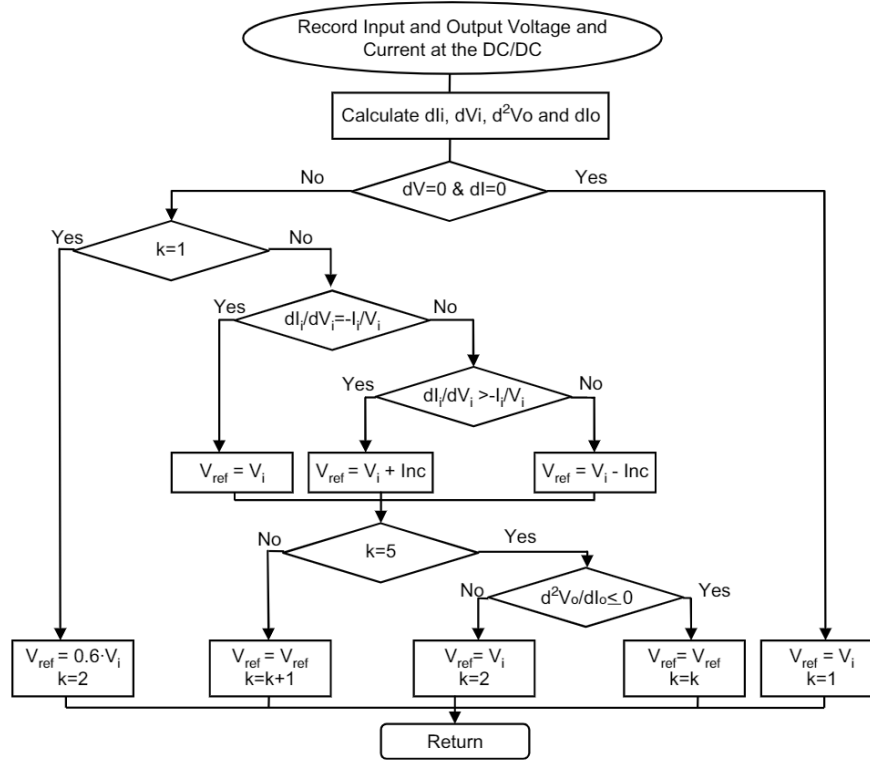


Figure 4.7: Control algorithm garcia-valverde [12]

Table 4.1: PV system Maximum Power Points (MPP)

| Irradiance [W/m <sup>2</sup> ] | PV System MPP [W] |
|--------------------------------|-------------------|
| 200                            | 1099              |
| 300                            | 1669              |
| 400                            | 2243              |
| 500                            | 2817              |
| 600                            | 3391              |
| 800                            | 4535              |
| 1000                           | 5671              |

figure the electrolyser voltage is shown and the power of both the PV and the electrolyser at the bottom. In this simulation can be seen that the power of the PV and Electrolyser is matched as the Maximum power from the PV which we can see in Figure 1.5 at  $100\text{W}/\text{m}^2$  irradiance the power is 535 W due to this the Electrolyser will work at 535 W at  $20^\circ\text{C}$  which results in the control algorithm to select the voltage of 223 V which can be seen in both Figure 4.13 and Figure 3.3. Figure 4.12 shows the zoomed version of the simulation at 6 seconds the irradiance is  $400\text{W}/\text{m}^2$  with the PV MPP being around  $2240\text{W} \approx 2243\text{W}$  which is the actual MPP which can be seen in Table 4.1 and Figure 1.5. Figure 4.12 shows that with this control also the MPP of the PV system is found without using a MPP tracker. On top of Figure 4.12 the voltage can be seen and the ripple was found to be  $\approx 0.01\%$ . This is due to over sizing the output capacitor. This capacitor was sized at  $10\text{E}-3\text{ F}$ . The inductor was also oversized at  $0.18\text{ H}$  resulting in a ripple of  $0.1\%$ .

This control continues for the different time periods and irradiance levels. But at time period  $t = 11\text{ s}$  the irradiance goes to  $800\text{W}/\text{m}^2$  and the maximum power point of the PV system is 4535 W but the electrolyser at temperature  $20^\circ\text{C}$  has a maximum working point of 4160 W and 260 V resulting in the control algorithm to select this voltage which causes the PV system power point to drop to this value of 4160 W. Also at an irradiance of  $1000\text{W}/\text{m}^2$  this happens as the power is 5671 W and the power that can be generated by the PV is higher than the maximum load from the electrolyser at that temperature resulting in the PV power dropping to the

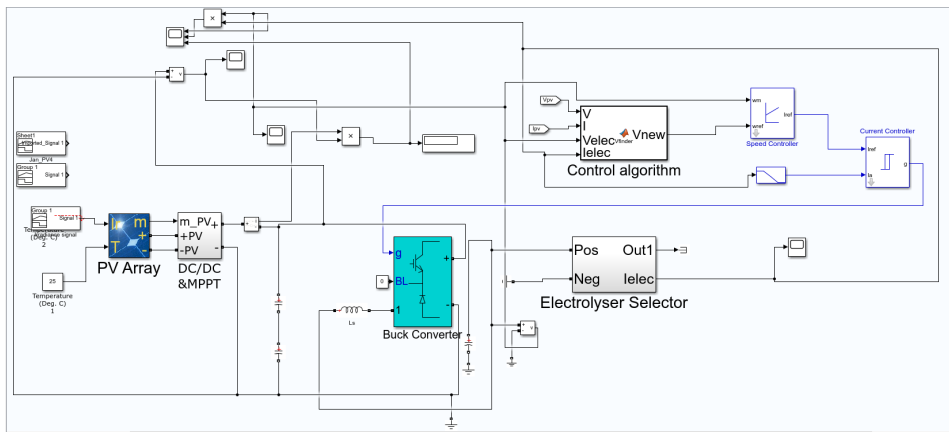


Figure 4.8: Simulink model with 2 converters : MPPT & Controller converters

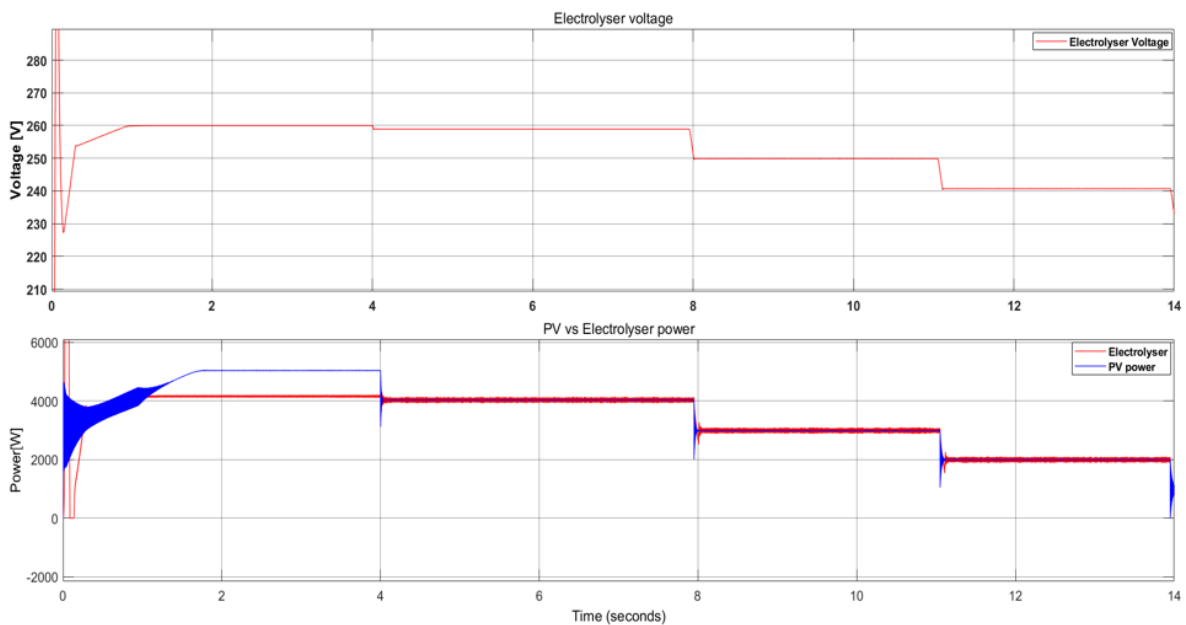


Figure 4.9: Simulink result of 2 converter model

maximum power that the electrolyser can use.

### 4.2.3. Constant Irradiance & Varying Temperature

Figure 4.14 shows the simulation where the different VI curves of the Electrolyser are used differentiating between the different temperatures. During this simulation the irradiance level is kept on  $800W/m^2$  with a maximum power point of  $4535W$  at  $60$  degrees this results in a Voltage level of  $245V$  which can be seen in Figure 3.3 timeperiod 0-4s and this also happens for temperatures of  $50^{\circ}C$ (4-8s),  $40^{\circ}C$ (8-12s) and  $30^{\circ}C$ (12-16s) as the maximum load of the electrolyser is higher than the maximum powerpoint of the PV system at that irradiance. But at  $20^{\circ}C$  the maximum working load of the electrolyser is  $4160W$  resulting in the power of the PV being matched to this value as can be seen in Figure 4.14 at timeperiod 16-20 s.

### 4.2.4. Varying Irradiance & Varying Temperature

Figure 4.15 shows the simulation in which both the irradiance changes and the temperature of the electrolyser. The irradiance changes follow Figure 4.11 and the Temperature changes in between these changes which can be seen in the Voltage levels of the electrolyser voltage curve on top of the Figure 4.15 at timeperiod 2 second the irradiance goes up resulting in the voltage going up to  $238V$  but at timeperiod 3 seconds the temperature of the electrolyser goes up to  $30^{\circ}C$  resulting in the voltage of the electrolyser going down but still the

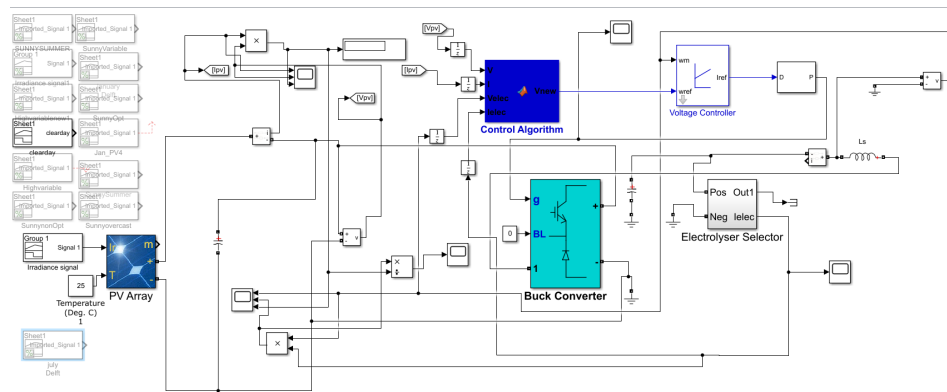


Figure 4.10: Simulink model 1 converter model

same power from is PV is consumed by the electrolyser. The same occurrence happens at time periods 6, 10, 14 and 18 seconds in which the temperature change results in the voltage change of the electrolyser.

### 4.3. PV system variation & day irradiance model

For the next simulations a more realistic simulation was done with a irradiance pattern resembling the irradiance during a day as seen in Figure 4.17. Also the temperature of the electrolyser was resembled as it would increase during the day just like in the case of the irradiance pattern. For the control a change was made, the change was to implement a power limit on the electrolyser. The power limit in this case should represent the electrolyser at its rated power in all temperatures/situations. The electrolyser rated power is rated at 5000 W.

The result of this simulation can be seen in Figure 4.18. On bottom of Figure 4.18 we see that with the irradiance increase during the day the PV power and also the electrolyser power increases, but at a certain time period the amount of power coming from the PV to the electrolyser hits 5 kW which is the limit and maximum power point (rated power) of the electrolyser. This stays constant but after some time the irradiance goes down again and goes lower than 5 kW and the PV power and Electrolyser power are matched again. On top of the Figure 4.18 we see the electrolyser voltage which fluctuates due to the irradiance changes and also due to the temperature changes which can be seen in Figure 4.16. When the irradiance is  $1000 \text{ W}/\text{m}^2$  and the electrolyser temperature goes to  $60^\circ\text{C}$ , the output voltage goes down as this temperature has a lower voltage for the same amount of power. From this result we see that the electrolyser works at its rated power from 12.5 seconds to 14.9 seconds (this can be seen as two and a half hours). This simulation with the same irradiance pattern can be simulated for different PV sizes to see how long the electrolyser would work for its rated power. This gives the advantages of having the electrolyser work at its rated power but also that when the irradiance is high there will be more extra unused power from the PV size. Figure 4.18 has a PV system sized for 6300W.

Figure 4.19 shows the simulation for PV system sizes at 7000 W and it can be seen that the electrolyser works at its rated power from 11.5 seconds to over 15.5 seconds which is an increase of 1.5 hours of the electrolyser working at its rated power but also seen in Figure 4.19 the blue line which is the PV power goes higher as it the size of the PV was increased. This extra power could be fed into a storage or grid if the model is further developed. Another simulation was done for PV size 8000 W in this case the electrolyser works at rated power from 11.25 to 15.75 so an increase of half an hour in regards to 7000 W.

#### 4.3.1. Winter & Summer day Delft

The following simulations were done in which the irradiance was changed to authentic irradiance data acquired from the KNMI dutch pv portal. The weather station selected was the closest one to delft (KNMI station rotterdam). This irradiance data is the average of the irradiance data for a specific period from 1991-2017 [44]. Two days were selected one in the summer (July 1) and one in the winter (January 1).

The simulations show that the control system has the ability to follow authentic irradiance data and follows the curve well.

#### 4.3.2. Clear day simulation

In this section the model is simulated with measured irradiance data for a clear day. To speed up the simulation the irradiance data is reduced to only looking at day time as the rest of the data is just  $0 \text{ W}/\text{M}^2$ , the

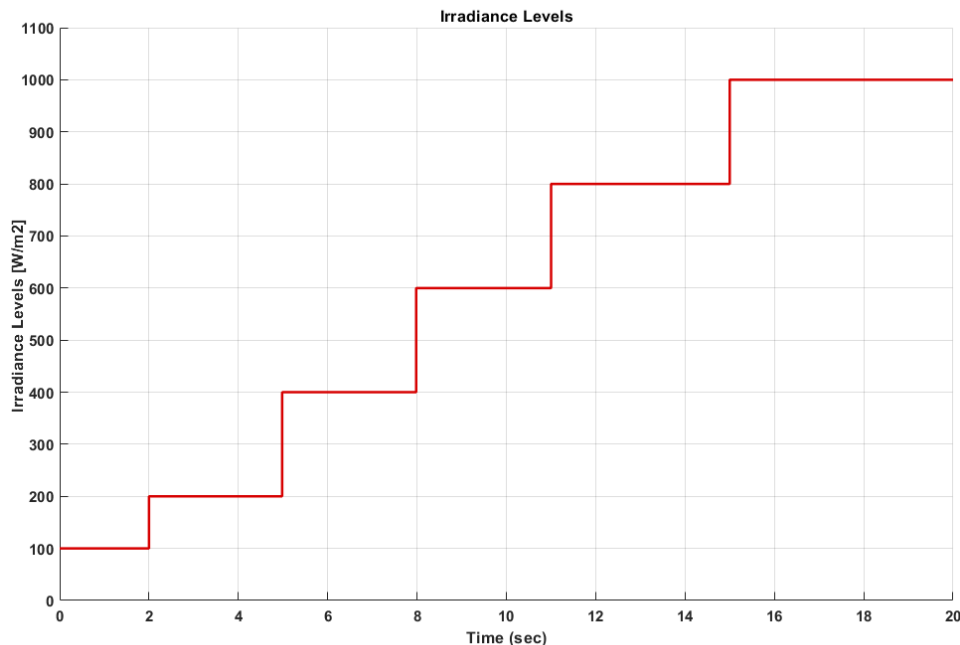


Figure 4.11: irradiance levels

Table 4.2: Converter+algorithm efficiency clear day (Voltage step vs time delay)

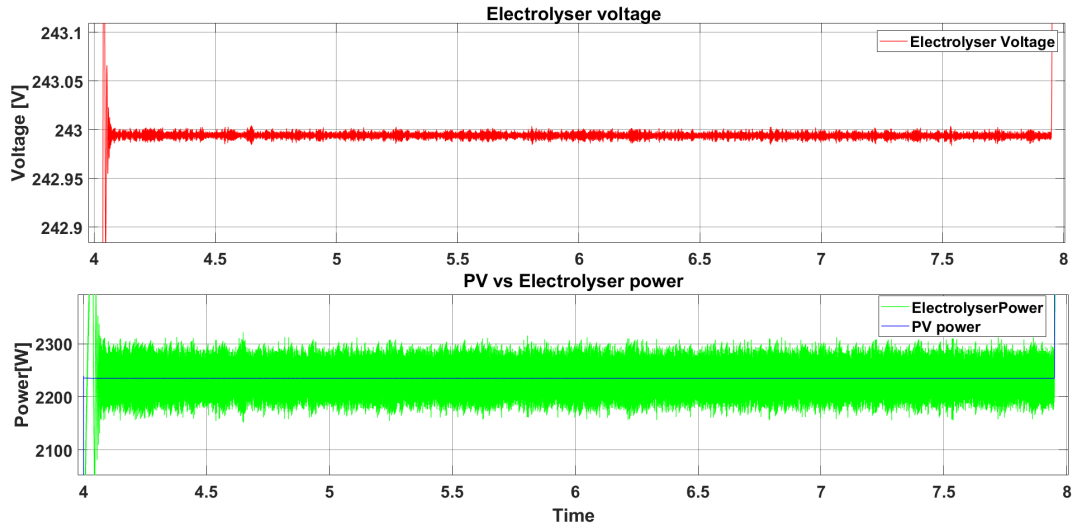
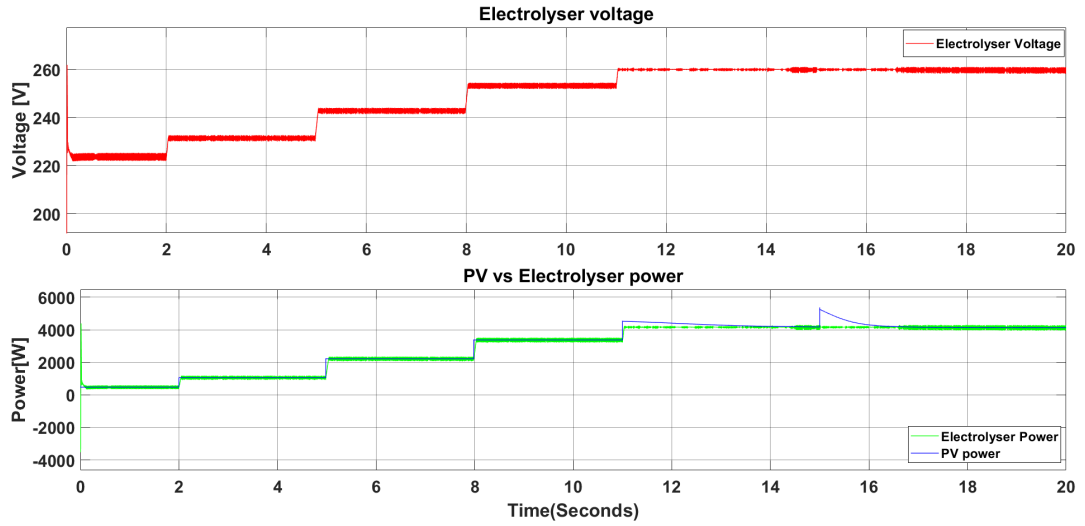
| Voltage steps[V] | Time delay [ms] |        |        |        |        |        |
|------------------|-----------------|--------|--------|--------|--------|--------|
|                  | 1               | 2      | 5      | 10     | 20     | 50     |
| 0.1              | 0.9842          | 0.9821 | 0.9824 | 0.9828 | 0.9831 | 0.9829 |
| 0.15             | 0.9809          | 0.9759 | 0.9784 | 0.9791 | 0.9797 | 0.9798 |
| 0.2              | 0.9785          | 0.9730 | 0.9750 | 0.9763 | 0.9765 | 0.9769 |
| 0.25             | 0.9755          | 0.9698 | 0.9717 | 0.9732 | 0.9736 | 0.9735 |
| 0.3              | 0.9725          | 0.9663 | 0.9688 | 0.9709 | 0.9708 | 0.9709 |
| 0.5              | 0.9589          | 0.9592 | 0.9590 | 0.9621 | 0.9618 | 0.9624 |

location where this data was taken is Cabauw, Utrecht, The Netherlands. The irradiance pattern can be seen in Figure 4.23. For this simulation the controller will have different delays and varying voltage steps it will take to find the right reference voltage. This is done to see the converter+algorithm or System efficiency. As mentioned in 4.2 the converter used for this one converter model simulations is the buck converter. This efficiency is calculated in the following way Equation 4.1 :

$$\eta = \frac{Pelectrolyser}{Ppvsystem} \tag{4.1}$$

A Steca 1010 MPP tracker used in the PVMD Lab takes voltage steps of 0.15V to find its MPP. The voltage range of the electrolyser that the controller will work in starts at 210 V and the maximum voltage is 260 V resulting in a voltage range 210-260V (40 V). Taking this into account the following voltage steps (deltaV) were selected for the controller 0.1, 0.15, 0.2, 0.25, 0.3, 0.5 V. Also to account for non-idealities time delays were also implemented into the system for the controller. The MPPT controller in [45] implemented time delays from 1 ms to 10 ms for its MPPT controllers. As it is a digital controller, time delay is not a parameter that can be predefined. This is because several factors have an effect on this delay such as computing time and communication [45]. The time delays implemented were 1, 2, 5, 10, 20, 50 ms.

In this model the passive components were modelled to be ideal resulting in no losses from these components as there was no series connected resistances. But the power electronic switch and diode were not ideal, these had some losses. The series resistance of both the diode and switch was found to be 1mΩ

Figure 4.12: Zoomed in  $400W/m^2$  Temperature  $20^\circ C$ Figure 4.13: PV vs electrolyser at  $20^\circ C$  power matching with changing irradiance

( $R_{diode}R_{switch}$ ). The losses in these two components can be calculated using equations 4.2 and 4.5 [46]. The highest amount of PV power received  $\approx 3730$  W using this and the voltage and current of the input and output of the converter the losses can be calculated. But the forward voltages were put on 0 V resulting in the equation for the Power loss in the diode 4.2 that the first term disappears [46]. The power electronic switch was selected to be a Mosfet although a IGBT switch could easily be implemented in the model.

The power lost in the diode was found to be  $\approx 15.30$  W and the power lost in the switch  $\approx 11.25$  W. This resulted in a efficiency lost of  $\approx 0.7\%$  at the highest amount power transferred through the converter.

$$P_{diode} = V_{forward}I_{avg} + R_{diode}I_{rms}^2 \quad (4.2)$$

$$I_{rmsdiode} = \sqrt{(1-D)\left(I_o^2 + \frac{\Delta I_L^2}{12}\right)} \quad (4.3)$$

$$\Delta I_L = \frac{V_s - V_oDTs}{L} \quad (4.4)$$

$$P_{switch} = R_{switch}I_{rms}^2 \quad (4.5)$$



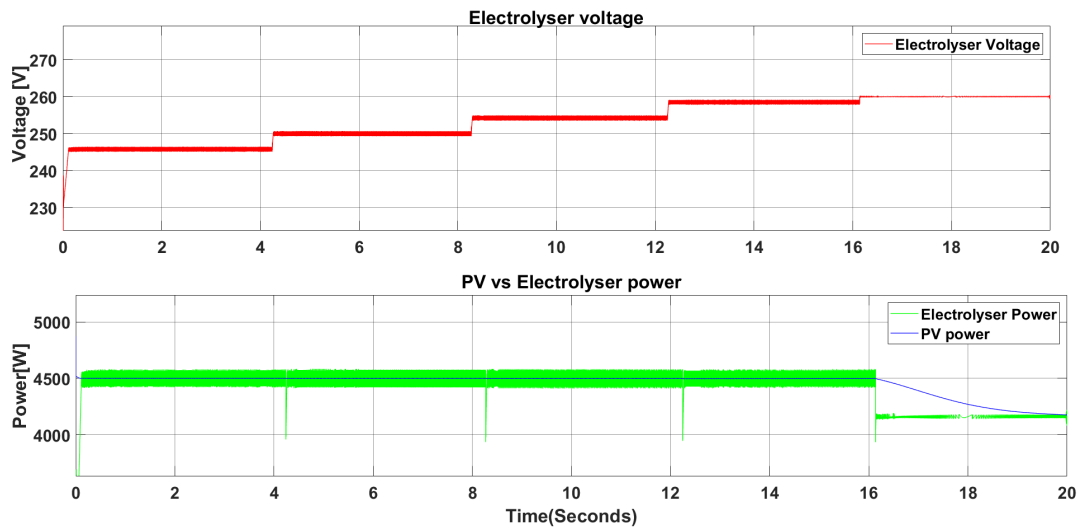


Figure 4.14: PV at  $800 W/m^2$  vs electrolyser at changing temperature

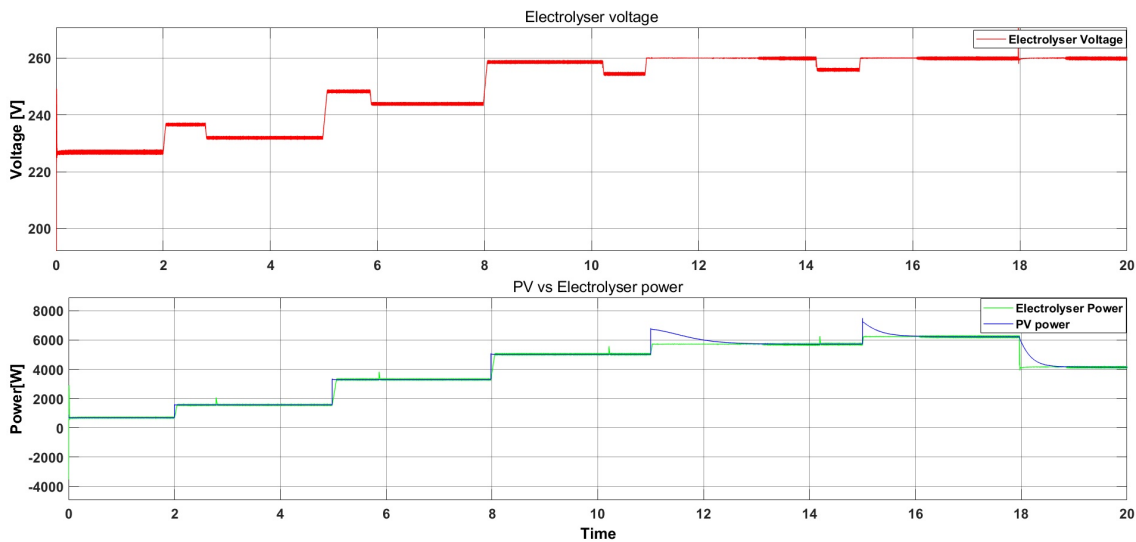


Figure 4.15: PV vs electrolyser power at changing temperature and changing irradiance

$$I_{rms\,switch} = \sqrt{D\left(I_o^2 + \frac{\Delta I_L^2}{12}\right)} \tag{4.6}$$

The simulation ran for 36 different combinations of time delays and voltage steps taken by the controller of the system in the one converter model using the buck converter. From Table 4.2 and Figure 4.24 the efficiency was highest for the voltage steps of 0.1 and a time delay of 1ms. If the voltage step taken is too large the accuracy of finding the exact reference voltage by the controller goes down [47]. The average efficiency of the Converter+Algorithm was calculated for all combinations of the Step size and Time delay implemented into the controller. These values can be found in Table 4.2. Also Figure 4.24 shows the the efficiencies for the different combinations. The results show that the efficiency is highest for a step size of 0.1 and time delay of 1ms, the efficiency was 98.4 %. These are the smallest time delay and the smallest voltage step of the different combinations. This is as expected as the accuracy of the controller is highest for the smallest voltage step [47]. The efficiency difference when changing the time delay for each voltage step is between 0.1 and 0.2 % but when changing the voltage step size the efficiency difference is between 1 and 2 %. Showing that variation in time delays gives less difference and that the controller is affected more by the voltage step. Concluding on this the recommended parameters are a voltage step size of 0.1V and time delay of 1ms.

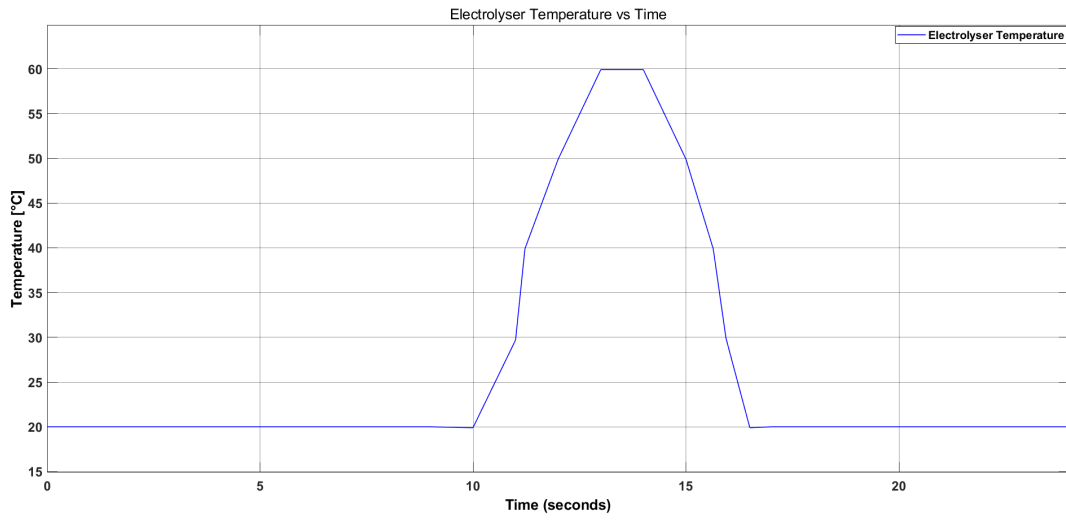


Figure 4.16: Electrolyser temperature changes for a day

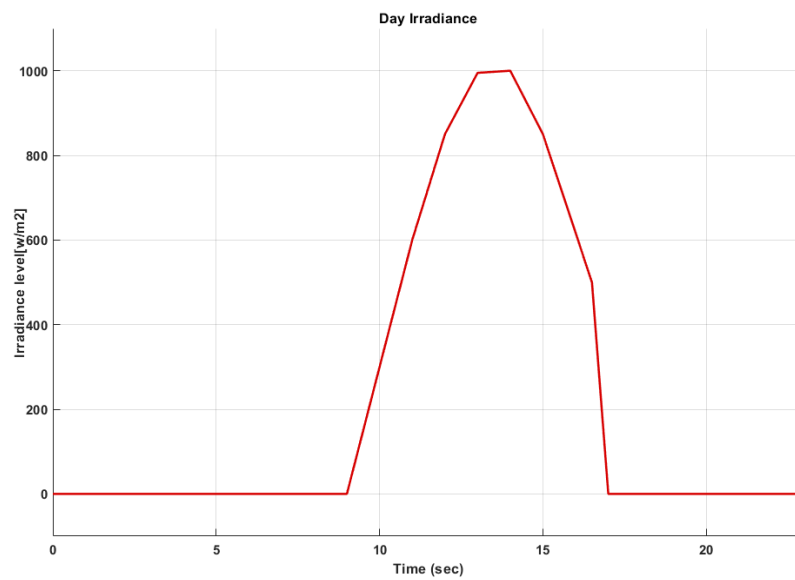


Figure 4.17: Irradiance levels in a day

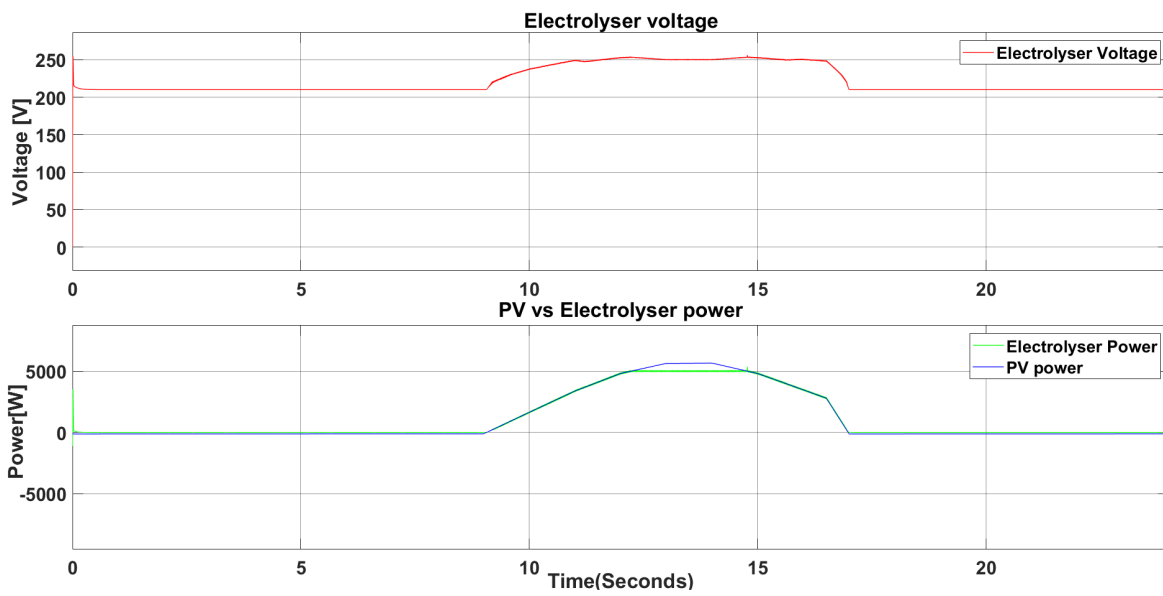


Figure 4.18: PV vs electrolyser power with new 5000W limit and hourly irradiance levels

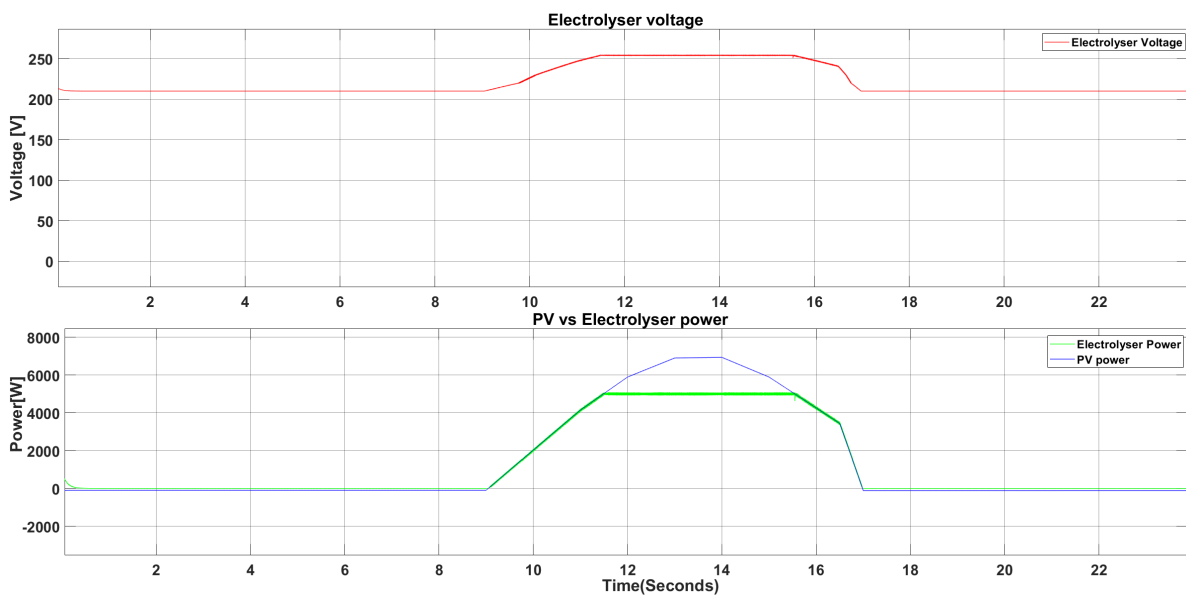


Figure 4.19: PV vs electrolyser power with 5000W limit and hourly irradiance levels PV sized at 7000 W

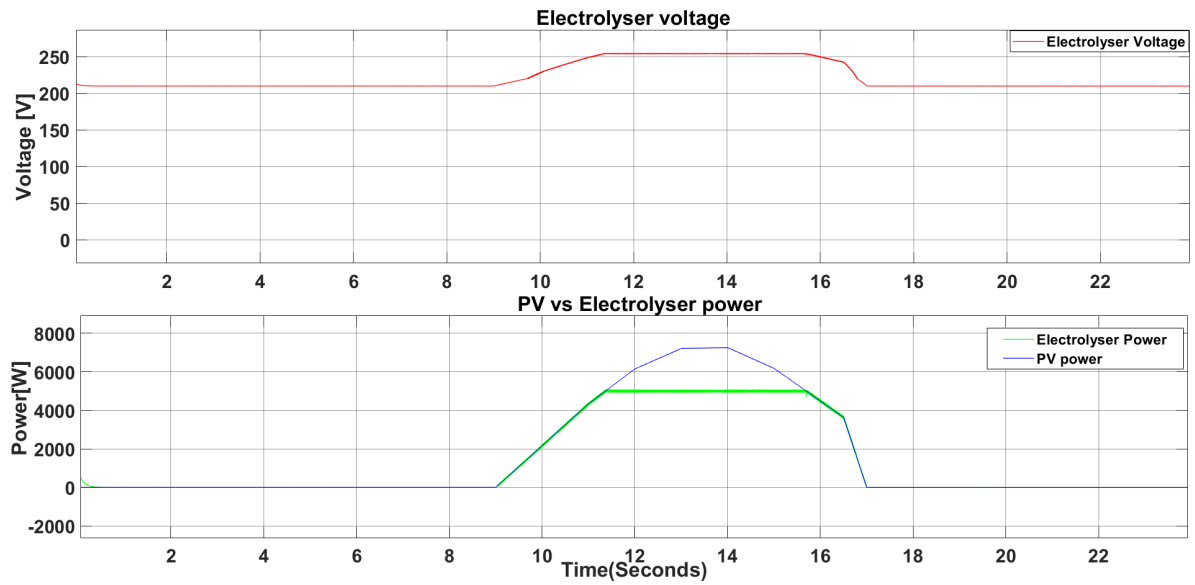


Figure 4.20: PV vs electrolyser power with 5000W limit and hourly irradiance levels PV sized at 8000 W

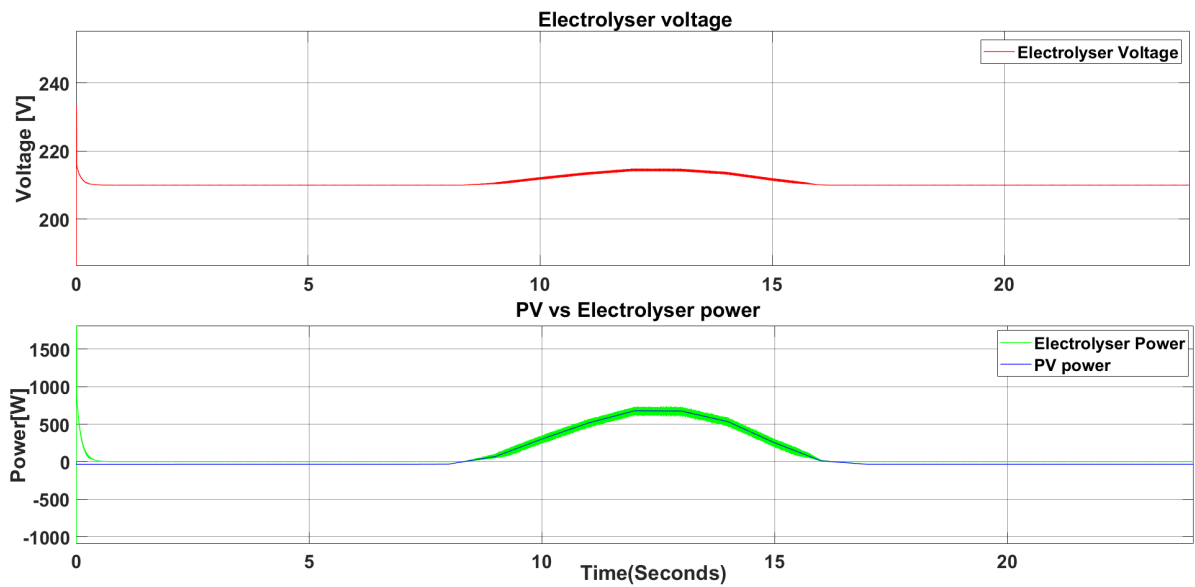


Figure 4.21: PV vs electrolyser power with 5000W limit Winter day delft

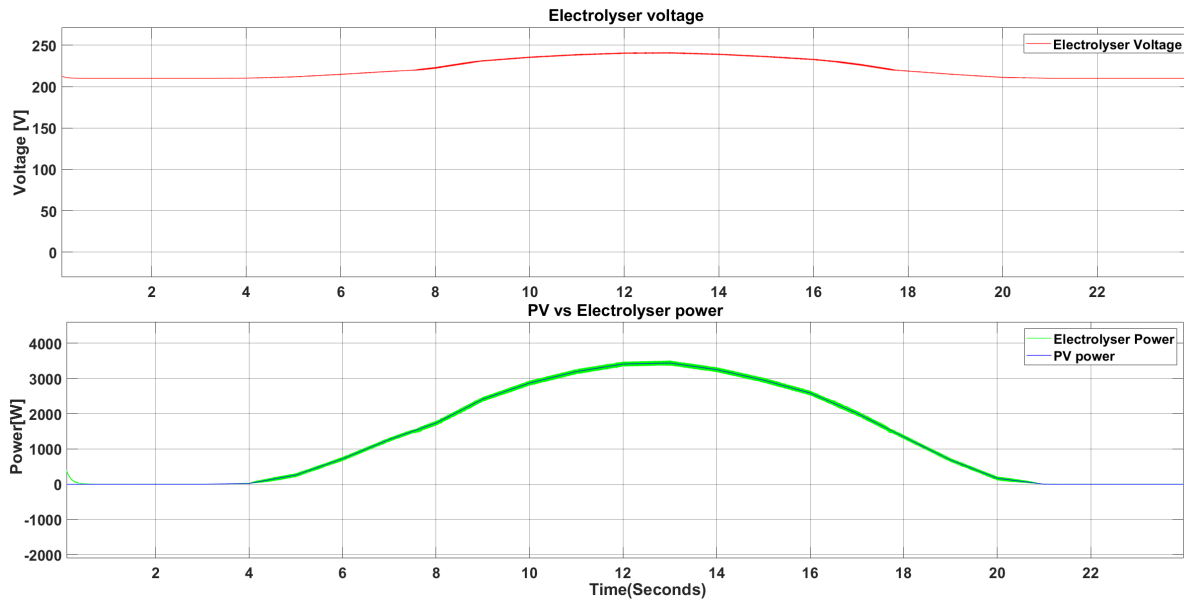


Figure 4.22: PV vs electrolyser power with 5000W limit Summer delft

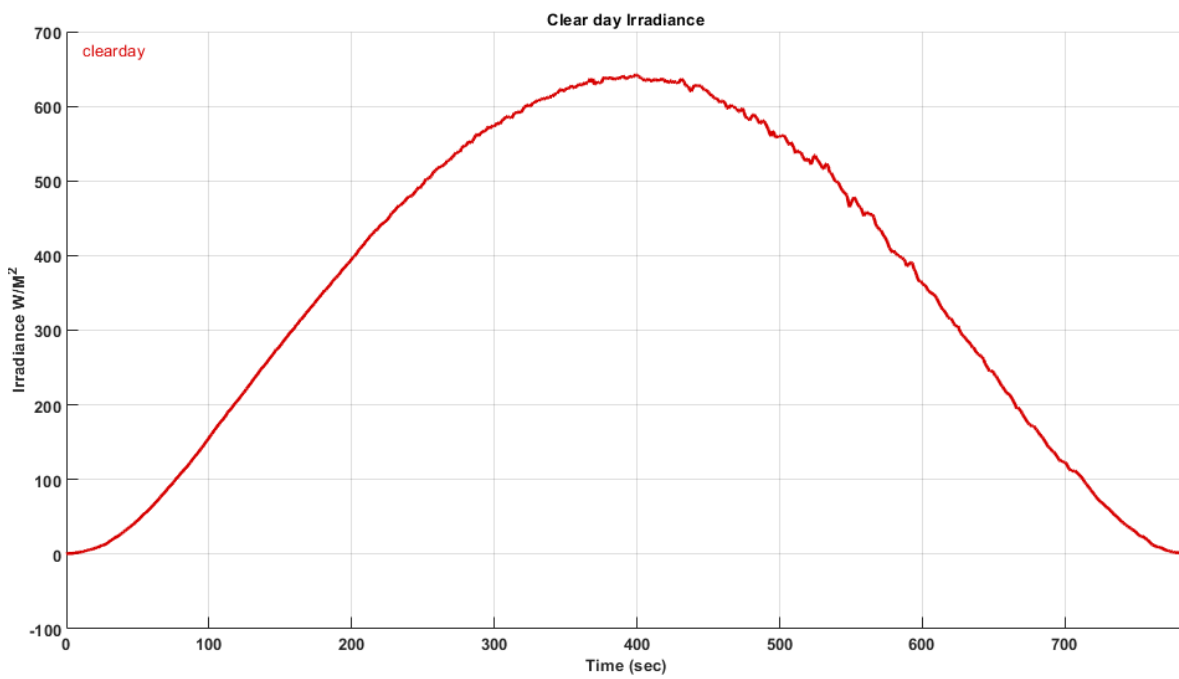


Figure 4.23: Irradiance pattern for a clear day

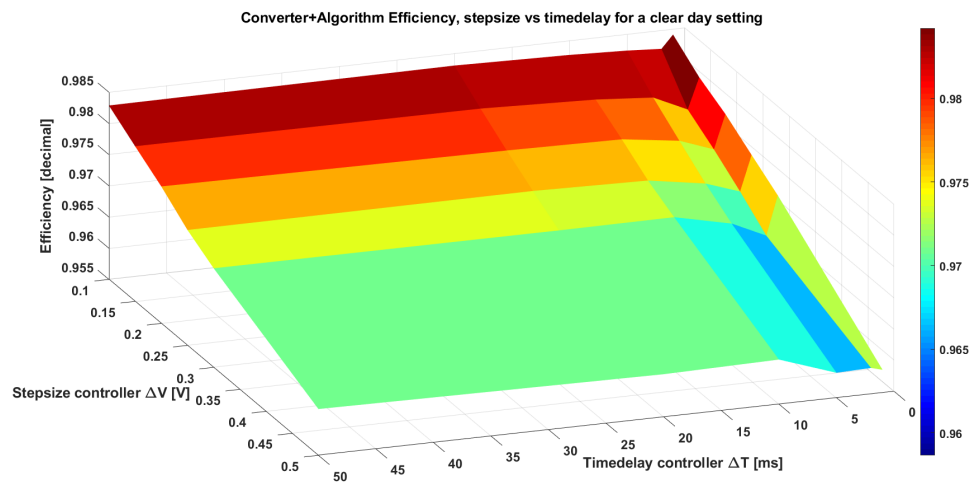


Figure 4.24: Converter+algorithm efficiency stepsize vs timedelay "clearday" (Buck converter)

# 5

## Conclusion & future recommendations

### 5.1. Conclusions

As the threat of climate change is still as present as ever, the need of the transition to more renewable energy sources from fossil fuels is as important as ever. The introduction of adding storage to the renewable energy system is one of the practices to introduce more renewable energy sources into the energy sector. For this project the idea was to connect a renewable energy source in this case PV system to an electrolyser system to produce hydrogen, which can be used later on. The main goals of this project were to select the most suitable DC-DC converters for the PV-electrolyser system, while also developing a control strategy that will optimize the efficiency/working points of this system. And from this project the following conclusions were drawn.

- The buck-boost converter was selected for the connection to the PV system for MPPT for its simplicity and ability to track the PV I-V curve.
- The 3-level interleaved buck converter was selected for the connection to the electrolyser system for the increased reliability and division of current ripples.
- A control strategy was developed for both two converters model as well for a one converter model.
- The control strategy was tested against multiple varying inputs such as changing irradiance and electrolyser temperature.
- A combination of different parameters (controller stepsize and time delay) were simulated to find the best performance.

To conclude the research objectives (Milestones) as mentioned in 1.4 were achieved and the research questions were answered. Indeed, the selected converters along with the designed control strategies achieved a sufficiently high efficiency according to the standards in the literature.

### 5.2. Recommendations

Improving on this model of a indirect connection of a PV system to an electrolyser system can be looked at from different angles such as other technical areas or even economic evaluations of the system sizes to optimize the hydrogen production and efficiency of the system.

- Other storage options (Batteries can be implemented to increase operation of the electrolyser at rated power.
  - Charge controller (converter) needed to charge (With the extra solar energy depending on the PV system size) and discharge the batteries (to increase operation time)
  - Control system adjustment to incorporate the storage system
- Implement grid connection to increase operation time of the electrolyser and feed the excess solar energy into the grid.

- Optimal Economic Evaluation of PV-storage-Electrolyser system to find the optimal size and costs of the system depending on the efficiency of the system.

Furthermore as mentioned in Chapter 2 soft switching can be used to increase the efficiency of the converter. Performing these different changes and evaluations will further improve this promising project and help expand the options for the energy transition in the upcoming years in battling climate change.



# Bibliography

- [1] IEA, "World energy outlook 2019," *World Energy Outlook*, 2019. DOI: 10.1787/caf32f3b-en.
- [2] P. Chandrasekhar and S. Reddy, "Optimum controlled full bridge lc resonant converter for electrolyser application," *Lecture Notes in Engineering and Computer Science*, vol. 2178, Oct. 2009.
- [3] B. Howard, *What the tesla powerwall home battery means: Inexpensive time-shifting for solar energy*, May 2015. [Online]. Available: <https://www.extremetech.com/extreme/204702-what-the-tesla-powerwall-home-battery-means-inexpensive-time-shifting-for-solar-energy>.
- [4] MIT, *Power distribution and energy storage*. [Online]. Available: <https://energy.mit.edu/area/power-distribution-energy-storage/>.
- [5] M. LITTLE, M. THOMSON, and D. INFIELD, "Electrical integration of renewable energy into stand-alone power supplies incorporating hydrogen storage," *International Journal of Hydrogen Energy*, vol. 32, no. 10-11, pp. 1582-1588, Nov. 2006. DOI: 10.1016/j.ijhydene.2006.10.035.
- [6] D. S. Gautam and A. K. Bhat, "A comparison of soft-switched dc-to-dc converters for electrolyser application," *2013 India International Conference on Power Electronics*, Jan. 2013. DOI: 10.1109/iicpe.2006.4685381.
- [7] sandia, *Single diode equivalent circuit models*. [Online]. Available: <https://pvpmc.sandia.gov/modeling-steps/2-dc-module-iv/diode-equivalent-circuit-models/>.
- [8] V. Guida, D. Guilbert, G. Vitale, and B. Douine, "Design and realization of a stacked interleaved dc-dc step-down converter for pem water electrolysis with improved current control," *Fuel Cells*, vol. 20, no. 3, pp. 307-315, 2020. DOI: 10.1002/fuce.201900153.
- [9] D. Guilbert, S. M. Collura, and A. Scipioni, "Dc/dc converter topologies for electrolyzers: State-of-the-art and remaining key issues," *International Journal of Hydrogen Energy*, vol. 42, no. 38, pp. 23966-23985, Sep. 2017. DOI: 10.1016/j.ijhydene.2017.07.174.
- [10] E. Hub, *4-different power converters*, Dec. 2017. [Online]. Available: <https://www.electronicshub.org/4-different-power-electronic-converters/>.
- [11] A. Tabanjat, M. Becherif, M. Emziane, D. Hissel, H. Ramadan, and B. Mahmah, "Fuzzy logic-based water heating control methodology for the efficiency enhancement of hybrid pv-pem electrolyser systems," *International Journal of Hydrogen Energy*, vol. 40, no. 5, pp. 2149-2161, 2015. DOI: 10.1016/j.ijhydene.2014.11.135.
- [12] R. GARCIAVALVERDE, C. MIGUEL, R. MARTINEZBEJAR, and A. URBINA, "Optimized photovoltaic generator-water electrolyser coupling through a controlled dc-dc converter," *International Journal of Hydrogen Energy*, vol. 33, no. 20, pp. 5352-5362, 2008. DOI: 10.1016/j.ijhydene.2008.06.015.
- [13] F. A. Inthamoussou, H. D. Battista, and R. J. Mantz, "New concept in maximum power tracking for the control of a photovoltaic/hydrogen system," *International Journal of Hydrogen Energy*, vol. 37, no. 19, pp. 14951-14958, 2012. DOI: 10.1016/j.ijhydene.2012.01.176.
- [14] S. Dahbi, A. Aziz, N. Benazzi, and M. Elhafyani, "Optimised hydrogen production by a photovoltaic - electrolysis system dc/dc converter and water-flow controller," *2015 3rd International Renewable and Sustainable Energy Conference (IRSEC)*, 2015. DOI: 10.1109/irsec.2015.7455129.
- [15] I. S. Ganeshan, V. Manikandan, V. Ram Sundhar, R. Sajiv, C. Shanthi, S. K. Kottayil, and T. Ramachandran, "Regulated hydrogen production using solar powered electrolyser," *International Journal of Hydrogen Energy*, vol. 41, no. 24, pp. 10322-10326, 2016. DOI: 10.1016/j.ijhydene.2015.05.048.
- [16] R. Babu and J. Henry, "A comparison of half bridge and full bridge isolated dc-dc converters for electrolysis application," *International Journal of Soft Computing and Engineering(IJSCE)*, pp. 37-42, 2011. DOI: 2231-2307.

- [17] Y. Yonezawa, M. Atsushi, H. Nakao, H. Takauchi, Y. Nakashima, H. Ebe, D. Yamashita, M. Sugiyama, Y. Ota, K. Nishioka, and et al., "Model-based development of solar-to-hydrogen conversion system with dynamic operating point control of multiple dc-dc converters," *2018 7th International Conference on Renewable Energy Research and Applications (ICRERA)*, 2018. DOI: 10.1109/icrera.2018.8566999.
- [18] A. Garrigós, J. Blanes, J. Carrasco, J. Lizán, R. Beneito, and J. Molina, "5kw dc/dc converter for hydrogen generation from photovoltaic sources," *International Journal of Hydrogen Energy*, vol. 35, no. 12, pp. 6123–6130, 2010. DOI: 10.1016/j.ijhydene.2010.03.131.
- [19] A. Garrigós, J. Lizán, J. Blanes, and R. Gutiérrez, "Combined maximum power point tracking and output current control for a photovoltaic-electrolyser dc/dc converter," *International Journal of Hydrogen Energy*, vol. 39, no. 36, pp. 20907–20919, 2014. DOI: 10.1016/j.ijhydene.2014.10.041.
- [20] P. Chandrasekhar and S. Rama Reddy, "Performance of soft-switched dc-dc resonant converter for electrolyzer," *2011 4th International Symposium on Resilient Control Systems*, Aug. 2011. DOI: 10.1109/isracs.2011.6016096.
- [21] S. Zorica, M. Vukšić, and T. Betti, "Design considerations of the multi-resonant converter as a constant current source for electrolyser utilisation," *International Journal of Electrical Power and Energy Systems*, vol. 111, pp. 237–247, 2019. DOI: 10.1016/j.ijepes.2019.04.019.
- [22] D. Hart, *Power electronics*. McGraw Hill, 2010.
- [23] v. kotak v.c and p. tyagi preti, *Dc to dc converter in maximum power point tracker*, Dec. 2013. [Online]. Available: <https://www.rroij.com/open-access/dc-to-dc-converter-in-maximum-power-point-tracker.pdf>.
- [24] M. Taghvaei, M. Radzi, S. Moosavain, H. Hizam, and M. Hamiruce Marhaban, "A current and future study on non-isolated dc-dc converters for photovoltaic applications," *Renewable and Sustainable Energy Reviews*, vol. 17, pp. 216–227, 2013. DOI: 10.1016/j.rser.2012.09.023.
- [25] M. Seyedmahmoudian, T. Kok Soon, E. Jamei, G. Thirunavukkarasu, B. Horan, S. Mekhilef, and A. Stojcevski, "Maximum power point tracking for photovoltaic systems under partial shading conditions using bat algorithm," *Sustainability*, vol. 10, no. 5, p. 1347, 2018. DOI: 10.3390/su10051347.
- [26] A. Joseph and J. Francis, "Design and simulation of two phase interleaved buck converter," in *National Conference on Recent Advances in Electrical & Electronics Engineering (NCREEE 2015)*, International Journal of Advanced Research in Electrical, Electronics and Instrumentation Engineering, vol. 4, International Journal of Advanced Research in Electrical, Electronics and Instrumentation Engineering, 2015, pp. 08–15.
- [27] N. Mohan, T. M. Undeland, and W. P. Robbins, *Power Electronics: Converters, Applications, and Design*. John Wiley and Sons, 2003.
- [28] R. Stull, *Isolated vs non-isolated power converters*, Dec. 2019. [Online]. Available: <https://www.cui.com/blog/isolated-vs-non-isolated-power-converters>.
- [29] D. Vinnikov, A. Andrijanovits, I. Roasto, and T. Jalakas, "Experimental study of new integrated dc/dc converter for hydrogen-based energy storage," *2011 10th International Conference on Environment and Electrical Engineering*, May 2011. DOI: 10.1109/eeeic.2011.5874667.
- [30] Y. Naimi and A. Antar, "Hydrogen generation by water electrolysis," *Advances In Hydrogen Generation Technologies*, 2018. DOI: 10.5772/intechopen.76814.
- [31] M. Ferrari, M. Rivarolo, and A. Massardo, "Hydrogen production system from photovoltaic panels: Experimental characterization and size optimization," *Energy Conversion and Management*, vol. 116, pp. 194–202, 2016. DOI: 10.1016/j.enconman.2016.02.081.
- [32] Ø. Ulleberg, "The importance of control strategies in pv-hydrogen systems," *Solar Energy*, vol. 76, no. 1-3, pp. 323–329, 2004. DOI: 10.1016/j.solener.2003.09.013.
- [33] Y.-t. Loong, M. Dahari, H.-j. Yap, and H.-y. Chong, "Development of a system configuration for a solar powered hydrogen facility using fuzzy logic control," *Journal of Zhejiang University SCIENCE A*, vol. 14, no. 11, pp. 822–834, 2013. DOI: 10.1631/jzus.a1300242.
- [34] J. GABRIELGARCIACLUA, R. JULIANMANTZ, and H. DEBATTISTA, "Hybrid control of a photovoltaic-hydrogen energy system," *International Journal of Hydrogen Energy*, vol. 33, no. 13, pp. 3455–3459, 2008. DOI: 10.1016/j.ijhydene.2007.12.046.

- [35] B. Yodwong, D. Guilbert, W. Kaewmanee, and M. Phattanasak, "Energy efficiency based control strategy of a three-level interleaved dc-dc buck converter supplying a proton exchange membrane electrolyzer," *Electronics*, vol. 8, no. 9, p. 933, 2019. DOI: 10.3390/electronics8090933.
- [36] I. Corporativa, *What is an electrolyser and why is it key to green hydrogen supply?* [Online]. Available: <https://www.iberdrola.com/sustainability/electrolyzer>.
- [37] M. Carmo, D. L. Fritz, J. Mergel, and D. Stolten, "A comprehensive review on pem water electrolysis," *International Journal of Hydrogen Energy*, vol. 38, no. 12, pp. 4901–4934, Apr. 2013. DOI: 10.1016/j.ijhydene.2013.01.151.
- [38] J. Brauns and T. Turek, "Alkaline water electrolysis powered by renewable energy: A review," *Processes*, vol. 8, no. 2, p. 248, Feb. 2020. DOI: 10.3390/pr8020248.
- [39] L. J. Nuttall, A. P. Fickett, and W. A. Titterton, "Hydrogen generation by solid polymer electrolyte water electrolysis," *Hydrogen Energy*, pp. 441–455, 1975. DOI: 10.1007/978-1-4684-2607-6\_31.
- [40] M. H. Shedid and S. Elshokary, "Hydrogen production from an alkali electrolyzer operating with egypt natural resources," *Smart Grid and Renewable Energy*, vol. 06, no. 01, pp. 14–25, Jan. 2015. DOI: 10.4236/sgre.2015.61002.
- [41] J. Klaus-Dieter, O. Isabella, A. H. Smets, van Swaaij René A.C.M.M, and M. Zeman, *Solar energy: fundamentals, technology and systems*. UIT Cambridge, 2016.
- [42] O. Isabella, *Pv systems components: Mpp tracking*, Jul. 2021.
- [43] A. Gaga, F. Errahimi, and N. Es-Sbai, "Design and implementation of mppt solar system based on the enhanced pamp;o algorithm using labview," *2014 International Renewable and Sustainable Energy Conference (IRSEC)*, 2014. DOI: 10.1109/irsec.2014.7059786.
- [44] PVMD. [Online]. Available: <https://pvportal-3.ewi.tudelft.nl/PVP3.1/Info/ModelExplanation.php>.
- [45] H. Zheng, S. Li, K. Bao, and D. Zhang, "Comparative study of maximum power point tracking control strategies for solar pv systems," *PES Tamp;D 2012*, Aug. 2012. DOI: 10.1109/tdc.2012.6281560.
- [46] T. Soeiro, *Semiconductor loss modeling*, Jul. 2021.
- [47] Ç. K. Gülnur and K. Aydın, "Step size strategies for the numerical integration of systems of differential equations," *Journal of Computational and Applied Mathematics*, vol. 236, no. 15, pp. 3805–3816, Mar. 2012. DOI: 10.1016/j.cam.2011.06.032.